GEORGIA INSTITUTE OF TECHNOLOGY
OFFICE OF CONTRACT ADMINISTRATION
SPONSORED PROJECT INITIATION

Date: 12/3/79

Project Title: RADC Post-Doctoral Program (C-E Systems)

Project No: A-2525 (Sub-project under E-21-626/Paris/EE)

Project Director: Mr. Hugh W. Denny

Sponsor: USAF, AFSC, Rome Air Development Center, Griffiss AFB, NY 13441

Agreement Period: From 10/1/79 Until 9/30/80 11/30/80
(Task Performance Period)

Type Agreement: Contract No. F30602-78-C-0120

Amount: $47,500 RADC
5,278 GIT (E-222-203)
$52,778 Total

Reports Required: Task Technical Report; Presentation Material
(For other reporting requirements see E-21-626)

Sponsor Contact Person (s):

Technical Matters

Contractual Matters
(thru OCA)

Dr. D. T. Paris
Director
School of Electrical Engineering
Campus
Extension 2902

Defense Priority Rating: DO-A7 under DMS Reg. 1

Assigned to: ETL/EMCG (School/Laboratory)

COPIES TO:

Project Director
Division Chief (EES)
School/Laboratory Director
Dean/Director—EES
Accounting Office
Procurement Office
Security Coordinator (OCA)
Reports Coordinator (OCA)
Library, Technical Reports Section
EES Information Office
EES Reports & Procedures
Project File (OCA)
Project Code (GTRI)
Other Dr. D. T. Paris/EE

GEORGIA INSTITUTE OF TECHNOLOGY
OFFICE OF CONTRACT ADMINISTRATION

SPONSORED PROJECT TERMINATION

Date: 4/23/81

Project Title: RADC Post Doctoral Program (C-E Systems)

Project No: A-2525

Project Director: D. E. Clark

Sponsor: USAF, AFSC, Rome Air Development Center

Effective Termination Date: 11/30/80

Clearance of Accounting Charges: 11/30/80

Grant/Contract Closeout Actions Remaining:

_ Final Invoice and Closing Documents
_ Final Fiscal Report
_ Final Report of Inventions
_ Govt. Property Inventory & Related Certificate
_ Classified Material Certificate
_ Other _____

Assigned to: ECSL/EMCD (~~School~~/Laboratory)

COPIES TO:

Project Director
Division Chief (EES)
School/Laboratory Director
Dean/Director–EES
Accounting Office
Procurement Office
Security Coordinator (OCA)
Reports Coordinator (OCA)
Library, Technical Reports Section
EES Information Office
Project File (OCA)
Project Code (GTRI)
Other _____

CA–4 (1/79)

FINAL TECHNICAL REPORT

HF/UHF LOW-LOSS NANOSECOND VARIABLE DELAY LINES

Circuitry for Interference Cancellation Systems

PROJECT A-2525

DONALD E. CLARK
WILLIAM R. HARDELL

Prepared for
ROME AIR DEVELOPMENT CENTER
GRIFFISS AIR FORCE BASE, NEW YORK 13441

Prepared by

ELECTRONICS TECHNOLOGY LABORATORY
ENGINEERING EXPERIMENT STATION
GEORGIA INSTITUTE OF TECHNOLOGY
ATLANTA, GEORGIA 30332

REPORT DOCUMENTATION PAGE

READ INSTRUCTIONS BEFORE COMPLETING FORM

1. REPORT NUMBER: RADC-TR
2. GOVT ACCESSION NO.:
3. RECIPIENT'S CATALOG NUMBER:

4. TITLE (and Subtitle): HF/UHF LOW-LOSS NANOSECOND VARIABLE DELAY LINES- Circuitry for Interference Cancellation Systems

5. TYPE OF REPORT & PERIOD COVERED: Final Technical Report 1 Oct. 79 - 30 Dec. 80

6. PERFORMING ORG. REPORT NUMBER: A-2525 (F)

7. AUTHOR(s): Donald E. Clark, William R. Hardell

8. CONTRACT OR GRANT NUMBER(s): F30602-78-C-0120

9. PERFORMING ORGANIZATION NAME AND ADDRESS: Georgia Institute of Technology, Engineering Experiment Station, Atlanta, GA 30332

10. PROGRAM ELEMENT, PROJECT, TASK AREA & WORK UNIT NUMBERS:

11. CONTROLLING OFFICE NAME AND ADDRESS: Rome Air Development Center (RBCT), Griffiss AFB, NY 13441

12. REPORT DATE: December 1980

13. NUMBER OF PAGES: 59

14. MONITORING AGENCY NAME & ADDRESS (if different from Controlling Office): Same

15. SECURITY CLASS. (of this report): UNCLASSIFIED

15a. DECLASSIFICATION/DOWNGRADING SCHEDULE: N/A

16. DISTRIBUTION STATEMENT (of this Report)

Approved for public release; distribution unlimited

17. DISTRIBUTION STATEMENT (of the abstract entered in Block 20, if different from Report)

Same

18. SUPPLEMENTARY NOTES

RADC Project Engineer: Wayne E. Woodward (RBCT)

19. KEY WORDS (Continue on reverse side if necessary and identify by block number)

Time Delay
Group Delay
Variable Delay Lines
Transmission Lines
Low-Loss Delay Lines
HF/UHF Delay Lines

20. ABSTRACT (Continue on reverse side if necessary and identify by block number)

Two delay line techniques are described: one for the HF band and the other for the UHF band. Both lines are similar in that they are broadband, low-loss, low-impedance, and nanosecond variable. The HF delay line is electrically variable and utilizes ceramic dielectric and ferrite materials in a coaxial line configuration. The UHF delay line is mechanically variable and utilizes coupled helical transmission lines.

FOREWORD

This report was prepared by the Electronics Technology Laboratory of the Engineering Experiment Station of the Georgia Institute of Technology. This work was conducted in response to Task N-0-5015 under Contact No. F30602-78-C-0120 of the RADC Post-Doctoral program. The described work was performed under the general supervision of D. W. Robertson, Director, Electronics Technology Laboratory, and H. W. Denny, Head, Electromagnetic Compatibility Branch. The principal investigator responsible for the project-level direction was Donald E. Clark, Senior Research Engineer. William R. Hardell, co-op student, performed most of the experimental work and model construction. Dr. Gordon R. Harrison's suggestions pertaining to the ferrite material selection are appreciated.

TABLE OF CONTENTS

LIST OF FIGURES

LIST OF FIGURES (continued)

FIGURES Page

LIST OF FIGURES (continued)

LIST OF TABLES

1.0 EXECUTIVE SUMMARY

1.1 BACKGROUND

Communication systems that are collocated as on an aircraft or at a ground station often interfere with each other when operated simultaneously. Interference cancellation systems (ICS) have been developed for use at transmitter and receiver antenna connections to reduce this type of interference. The ICS is a balanced bridge configuration with a radiated path between two antennas and a conducted path between a transmitter output and a receiver input. Within a controller located in the conducted path, a signal is synthesized to cancel at the receiver input the interfering signal that couples via the radiated path. Since the ICS is a balanced bridge arrangement, any movement between antennas in the radiated path that is not corrected in the conducted path results in a reduction of the cancellation. On aircraft installations the flexing of the wing antennas results in a varying radiated path that is not compensated for in the conducted path. To provide the compensation required for path changes, an adaptive time delay circuit or device is required in the conducted path to correct for the varying radiated path length. The objective of this program is to study and investigate techniques and devices for use in an adaptive time delay circuit. Time delay circuitries usable within the HF (2-30MHz) and UHF (225-400 MHz) bands are to be investigated.

1.2 SUMMARY

Two time delay line techniques have been studied and investigated. Both techniques are similar in that they are broadband, low-loss, low-impedance (50 ohms), and nanosecond variable, i.e., offers nanosecond resolution. For the HF band, the delay line is electrically variable and utilizes ceramic dielectric and ferrite materials in a coaxial line configuration. The UHF band delay line is mechanically variable and utilizes coupled helical transmission lines.

Experimental models of the two delay lines have been designed and constructed. The design principles and the construction details of the two

delay lines are given. Characteristics such as time delay variation, insertion loss, input impedance, VSWR, power-handling capability, and intermodulation products have been measured and reported in graphical or table form.

1.3 CONCLUSIONS

Experimental results for the ferrite-loaded helical line were very good, and this technique is a viable candidate for the HF delay line. The characteristics of the line can be improved through better construction techniques.

The experimental results for the coupled helical line were encouraging. Additional development is needed to realize its potential as a candidate for the UHF delay line. In particular, improved coupling and termination techniques need to be investigated.

2.0 DESIGN OBJECTIVES

The delay lines are to be designed so that they may be inserted with minimum modification in the conducted path of an ICS. The lines should have a flat response in amplitude and a linear phase response (constant time delay) with respect to the input. Any nonlinearity will cause distortion on the synthesized signal in the conducted path. Since the distortion cannot be cancelled, it limits the achievable ICS cancellation. Signal bandwidths of at least 3 KHz need to be accommodated. The other performance objectives for the delay line techniques are:

Frequency	HF (2-30 MHz) UHF (225-400 MHz)
Time Delay Variation	10 nanoseconds
Time Delay Resolution	$\pm$0.01 nanosecond
Time Delay Variation Rate	15-20 Hz
Insertion Loss	7 dB or less
Power Capability	50 watts average
Input Impedance	Nominal 50 ohms
Intermodulation Products	55 dB down from input

3.0 CANDIDATE DELAY LINE TECHNIQUES

A comprehensive survey of the technical literature and manufacturer information pertaining to variable time delay techniques has been completed and reported on during a previous Air Force sponsored program [1]. It was found that numerous time delay techniques had been investigated. However, many of the time delay methods were not suitable for this program's design objectives. The reasons are:

(1) Many of the methods have high insertion or conversion losses on the order of 25-50 dB.

(2) Other methods had long time delays on the order of microseconds and were not capable of nanosecond variability.

(3) Some methods were narrowband and required tuning to operate over a frequency band.

(4) Nonlinear devices such as diodes or mixers which produce undesired high-level intermodulation products when operated at high power levels were used in some methods.

(5) The modes, e.g. spin waves, used to produce time delay in many methods do not exist in the lower frequency ranges.

Based on the survey evaluation and further investigations early in this program, two delay line techniques were selected for study and investigation per the design objectives. For the HF band, a coaxial transmission line with a helical center conductor wound on a ferrite rod embeddded in a high-permittivity dielectric material was chosen. The time delay through the line is varied by applying a dc magnetic field to change the permeability of the rod. Experimental results obtained during the previously mentioned Air Force sponsored program showed the feasibility of this type of variable delay line. To permit brevity, this line will be referred to as the ferrite-loaded helical line. For the UHF band, a coupled helical transmission line was selected. The line consists of a metallic helix wound on a dielectric form. The axial propagation velocity down the helix is a fraction of the velocity along the helical conductor. The time delay through the helical transmission line is varied by mechanically changing the coupled path length. Early in this program, calculations and review of previous investigations

showed the feasibility of this line per the design objectives.

The following sections report in detail on the ferrite-loaded helical line and the coupled helical line. The design principles, model construction, and experimental results are discussed. For a review of time delay relationships pertinent to the discussions, refer to Appendix A.

4.0 HF VARIABLE DELAY LINE

The ferrite-loaded helical line was investigated by Megla and others [2] in 1968. Their application of the line was for fixed time delays. Nevertheless, Megla's design equations and design example are used as a basis for this investigation of variable delay lines.

4.1 DESIGN PRINCIPLES FOR THE HF DELAY LINE

For the ferrite-loaded helical line, a coaxial section is used with the center conductor replaced with a helix on a ferrite rod and a high-permittivity dielectric material is used to fill the annular space. This configuration increases both the inductance (L) and capacitance (C) per unit length as compared to the usual coaxial line construction. The time delay per unit length, which is equal to $\sqrt{LC}$, is thus increased. The characteristic impedance of the line is equal to $\sqrt{L/C}$, and low-impedance is achieved by using a high-permittivity dielectric in the annular space to increase the capacitance C.

The complete solution for the propagation characteristics through the ferrite-loaded helical line requires a solution of the wave equation. However, the line may be characterized in terms of L and C since the wavelengths of interest are greater than the significant line dimensions. Simplifying assumptions are made to approximate L and C. The inductance is taken to be the sum of the inductance of a coaxial line and the inductance of the helix. Thus the inductance is expressed as:

$$L = L_c + L_h \tag{1}$$

where

L_c = coaxial line inductance per unit length
L_h = helix inductance per unit length.

Based on this assumption, Megla gives the inductance per unit length as:

$$L = \frac{\mu_{rc}\,\mu_o}{2\pi} \ln d/b \left[1 + \frac{(N\pi b)^2}{2\,\mu_{rc} \ln d/b} \cdot \left(\frac{\mu_{rh}(d^2/b^2 - 1)}{(d^2/b^2 - 1) + \mu_{rh}/\mu_{rc}} \right) \right] \quad (2)$$

where

μ_{rc} = permeability of the coaxial dielectric

μ_{rh} = permeability of ferrite material

μ_o = magnetic constant = $4\pi \times 10^{-7}$ henrys/meter

d = outer diameter of dielectric material

b = outer diameter of helix

N = helix turns per unit of length.

The capacitance of the line is approximated by replacing the helix with a continuous conductor which is an accurate model for small pitch angles. With this approximation, the capacitance is simply that of a coaxial line and is equal to:

$$C = \frac{2\pi\,\varepsilon_{rc}\,\varepsilon_o}{\ln d/b} \quad (3)$$

where

ε_{rc} = relative permittivity of coaxial dielectric

ε_o = electric constant = 8.854×10^{-12} farads/meter.

Equations 2 and 3 are the basic equations needed to design the ferrite-loaded helical line. The characteristic impedance is given by:

$$Z_h = [L/C]^{1/2} \quad (4)$$

where Z_h is in ohms. The time delay per unit length is given by:

$$t_d = [LC]^{1/2}. \tag{5}$$

Equations 2, 3, 4, and 5 were used to design the variable ferrite-loaded helical line. First the diameter ratio was chosen for a characteristic impedance of 50 ohms when the ferrite material permeability μ_{rh} was at its mid-range. (The variability of the ferrite material is discussed in the next section.) Next the time delay variation was calculated by the equation:

$$\Delta t_d = (t_d)_{H=0} - (t_d)_{H=max} \tag{6}$$

where

Δt_d = time delay variation in seconds per unit length

$(t_d)_{H=0}$ = time delay for unmagnetized ferrite in seconds per unit length

$(t_d)_{H=max}$ = time delay for saturated ferrite in seconds per unit length.

The design equations for the ferrite-loaded helical line do not account for the air gaps between the ferrite rod and the ceramic dielectric and between the ceramic dielectric and the outer conductor. These air gaps reduce the effective permittivity of the line and in turn the line capacitance. The importance of minimizing the air gaps is evident when considering the two-dielectric capacitor shown in Figure 1, which may be considered as an "unrolled" model of the coaxial line. The effective dielectric constant of the material is:

$$\frac{1}{\varepsilon_{eff}} \approx \frac{1}{\varepsilon_2} + \frac{\ell_1}{\ell_2} \tag{7}$$

where

ε_{eff} = effective dielectric constant

ε_2 = dielectric constant of material

ℓ_1 = air gap thickness in inches

ℓ_2 = dielectric material thickness in inches.

As an example consider a two-dielectric capacitor with an air gap ($\varepsilon_1 = 1$), $\varepsilon_2 = 200$, $\ell_1 = 0.001$ inches and $\ell_2 = 0.5$ inches. The effective dielectric constant is found to be 143, a large reduction from the 200 dielectric constant.

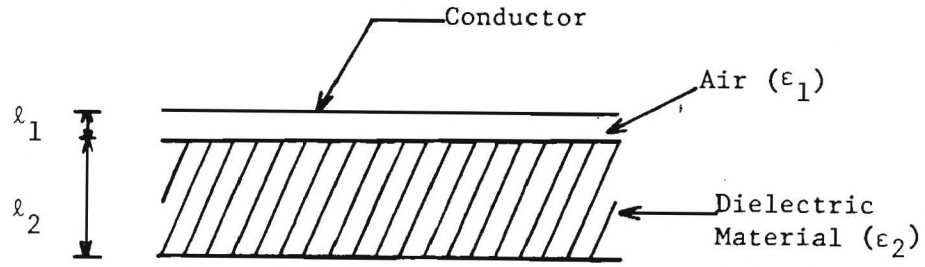

Figure 1. Two-Dielectric Capacitor

Another factor in the design of the ferrite-loaded helical line is the power-handling capability. Approximating the helical line as a lossless coaxial line, the gradient [3] at the surface of the center conductor is:

$$E = \frac{5.37}{d}\left(\frac{\text{VSWR } P_{KW}}{Z_o\ \varepsilon}\right)^{1/2} \qquad (8)$$

where

E = gradient in peak volts/mil

d = diameter of center conductor in inches

VSWR = voltage standing wave ratio

Z_o = characteristic impedance in ohms

ε = dielectric constant

P_{KW} = power in kilowatts.

The loss of the ferrite-loaded helical line also determines the power-handling capability since a fraction of the input power is absorbed as loss. Since the losses increase with frequency, the power-handling capability is also a function of frequency. The absorbed power is dissipated as heat with a rise in temperature of the materials within the line. High temperatures may change the material properties, and thus the delay line characteristics. To minimize these changes, the line may be cooled.

4.2 MATERIAL SELECTION

The material selected for construction of the ferrite-loaded helical line ultimately determines the line characteristics. Before discussing the material, first consider the behavior of a ferrite material [4] when a magnetic field is applied. Figure 2(a) shows the typical complex permeability of an unmagnetized ferrite as a function of frequency, and such data are referred to as the initial permeability spectra [5]. The permeability changes that are important for the ferrite loaded helical line are due to domain wall motions and not the gyromagnetic effects that occur at higher frequencies. For a partially magnetized ferrite as shown in Figure 2(b), the inductivity (μ') and the magnetic loss factor (μ'') decrease in amplitude. When the ferrite is saturated, as shown in Figure 2(c), the inductivity is unity and the magnetic loss factor is very small. The change of permeability with the applied dc magnetic field is the mechanism that produces the variable delay in the ferrite-loaded helical line. Thus to achieve large time delay variability, a material with high initial permeability should be selected. However, a trade-off must be made between high initial permeability and loss. This trade-off is evident in Figure 3. Complex permeabilities of three ferrite materials A, B, and C are shown. For ferrite A the inductivity is the highest but so is the magnetic loss factor. For ferrite C the inductivity is less and the magnetic loss factor is less. Notice that the frequency range for ferrite C is greater.

Based on the trade-off considerations, a nickel-cobalt ferrite type TT2-101 supplied by Trans-Tech, Gaithersburg, Maryland was selected for the ferrite-loaded helical line. The TT2-101 has an initial complex permeability of 19 + j0.15 at 30 MHz. The loss of the material increases

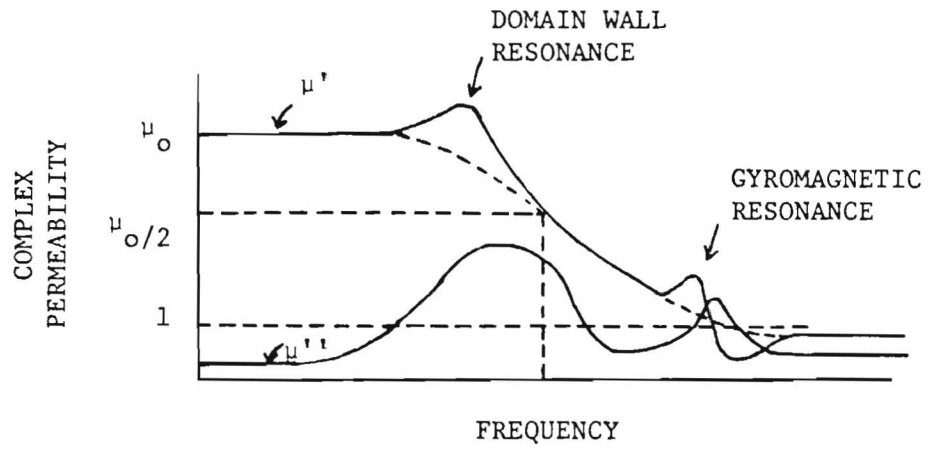

(a) UNMAGNETIZED FERRITE

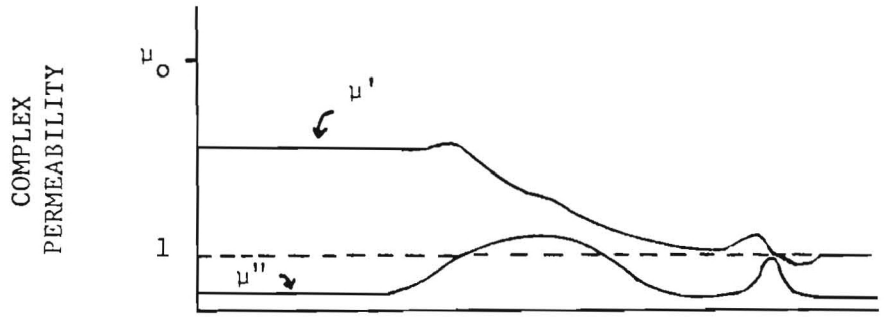

(b) PARTIALLY MAGNETIZED FERRITE

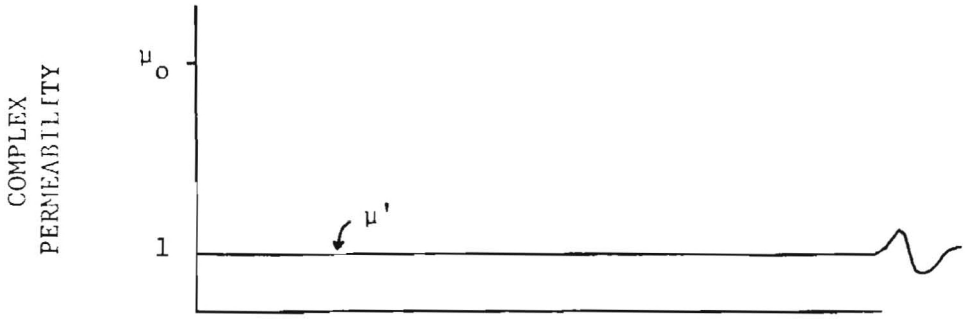

(c) SATURATED FERRITE

Figure 2. Predicted Behavior of Ferrite Material with Frequency and Applied DC Magnetic Field

rapidly for frequencies above 100 MHz. The dielectric constant of the material is 12.8, and the dielectric loss tangent ($\tan\delta$) is less than 0.0025. The material's Curie temperature is 585 degrees C.

Desirable properties of the dielectric material for use in the annular space of the ferrite-loaded helical line are a high dielectric constant and a low dielectric loss tangent. The high dielectric material increases the capacitance and in turn the time delay. The dielectric material selected was MCT-140 also supplied by Trans-Tech. MCT-140 is a ceramic with a calcium titanate composition with a dielectric constant of 140 ± 10% and a dielectric loss tangent less than 0.002. Handbook data [3] states the dielectric strength of calcium titanate as 100 volts/mil.

4.3 MODEL CONSTRUCTION FOR THE HF DELAY LINE

Two design models of the ferrite-loaded helical line were constructed. For discussion purposes the models are designated as Design Models 1 and 2. Drawings and design data for the two models are given in Figure 4. Design Model 1 is the shorter line and utilized a 2.25 inch ferrite rod. Design Model 2 is the longer line and has a 6.0 inch ferrite rod. Figure 5 is a picture of the Design Model 2 and the solenoid used to generate the applied dc magnetic field.

Two solenoids were used. The solenoid for Design Model 1 was 3.5 inches long with an inner diameter of 1.25 inches. The solenoid had 1500 turns of 22 AWG enamel-coated copper wire. The Design Model 2 solenoid was 7.5 inches long with an inner diameter of 0.75 inches. This solenoid had 1250 turns of 22 AWG enamel-coated copper wire. The method used to calibrate the solenoids is discussed in Appendix B.

The coaxial line construction has several inherent advantages: (1) the line is shielded from external electromagnetic interference (EMI), (2) stray capacitance and inductance are minimized, and (3) close coupling occurs between the applied dc magnetic field and the ferrite rod.

Several mechanical constraints were encountered during the construction of the design models. First, a more precise construction technique would entail the machining (diamond grinding is required) of a helix form into the ferrite rod. The entire rod would next be metallized, and the excess metal machined off to produce a metallic helix embedded in the ferrite rod.

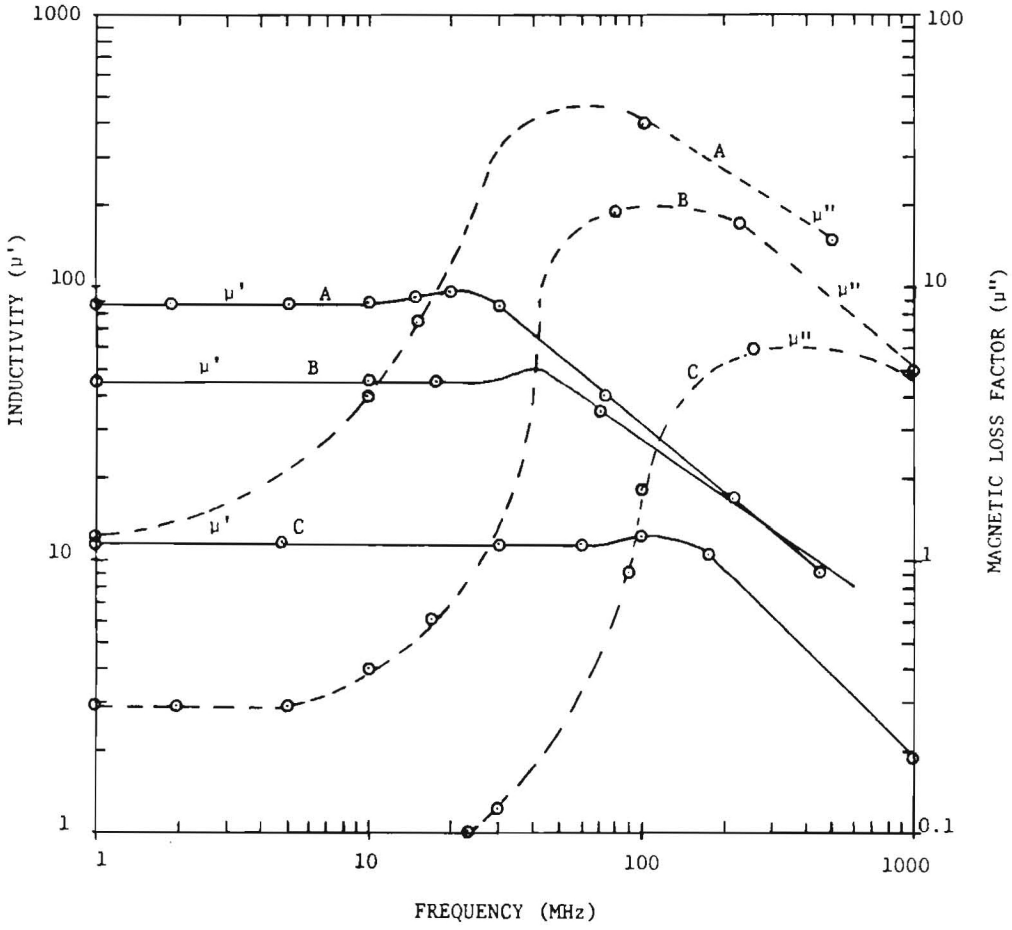

Figure 3. Typical Complex Permeability for Ferrite Materials (A, B, and C) as a Function of Frequency

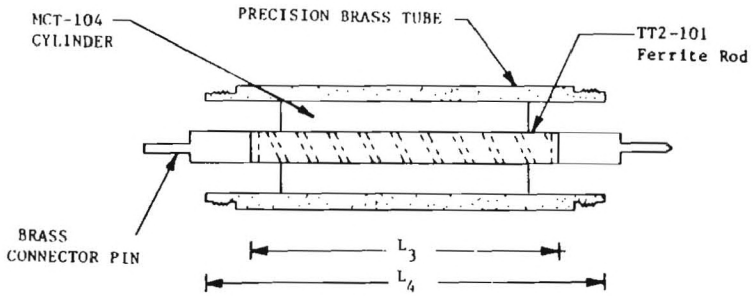

(a) Design Model 1 Construction

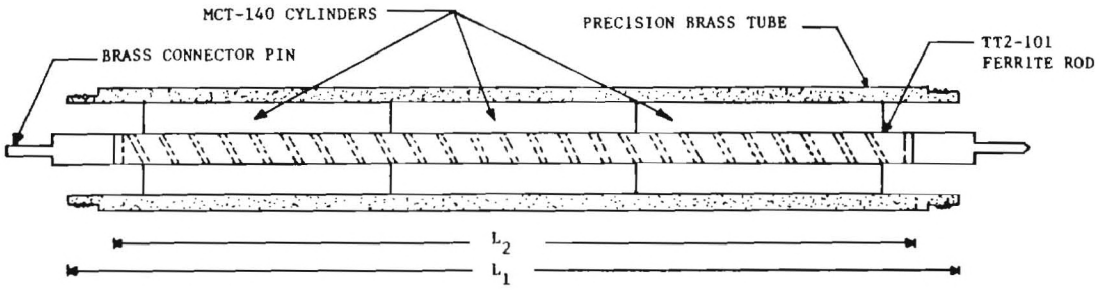

(b) Design Model 2 Construction

DESIGN DATA FOR THE FERRITE-LOADED HELICAL LINES

Description	Dimensions	Supplier
Precision Brass Tube	0.5625 inches ± 220 microinch ID 0.74 ± .015 inch OD 6.5 inch ± .015 inch length (L_1) 2.75 inch ± .015 inch length (L_3)	GEN RAD PN 0900-9509
MCT-140 Ceramic Dielectric	0.256 inch ± 1 mil ID 0.560 inch ± 1 mil OD 1.850 inch ± 1 mil length	TRANS-TECH
TT2-101	0.250 inch ± 1 mil Dia. 6.0 inch ± 1 mil length (L_2) 2.25 inch ± 1 mil length (L_4)	TRANS-TECH
Aluminum Foil Tape Helix	2 mil thick x 50 mil wide 50 turns/6 inches	STOCK
Brass Connector Pins	0.25 inch D x 0.5 inch L 0.12 D x 0.5 inch L	STOCK

Figure 4. Construction and Design Data for the Ferrite-Loaded Helical Lines

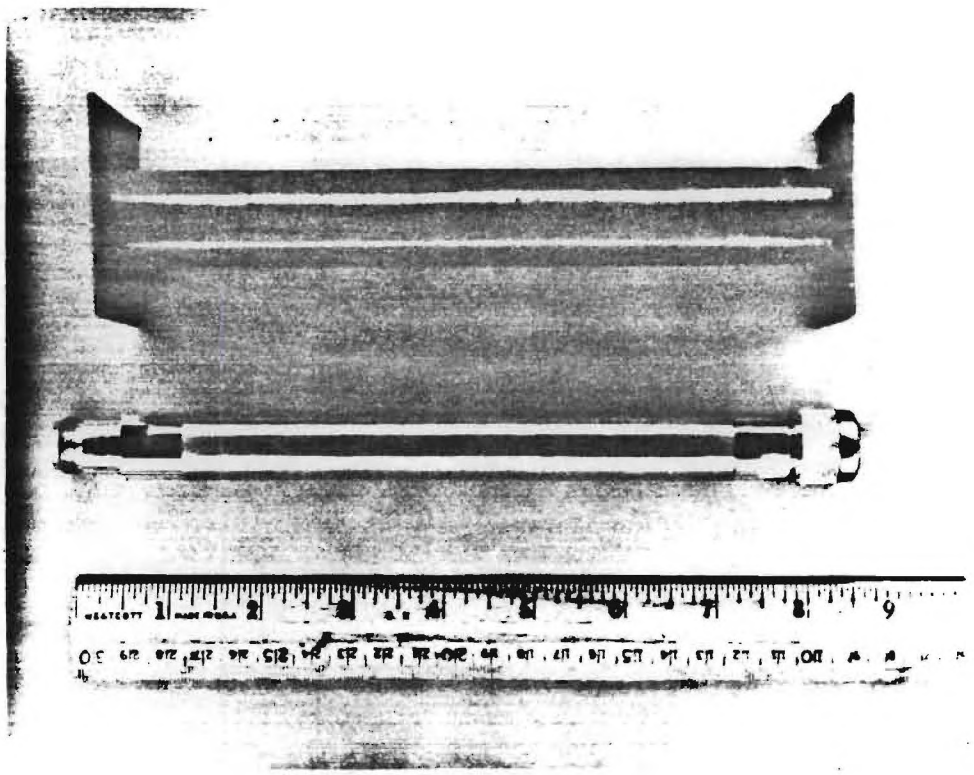

Figure 5. Photograph of Ferrite-Loaded Helical Line

Such construction with close tolerances minimizes the air gap between the ferrite rod and the ceramic cylinders. After discussions with manufacturers of ferrite components, it was found this was not a common machining operation, and the initial tool set-up costs were therefore expensive. Based on this information, the alternative of using an aluminum tape helix wound on the ferrite rod was chosen. Of course, this procedure results in a larger air gap. Another constraint encountered was in the machining of the ceramic dielectric cylinders. For Design Model 2, a 6-inch long ceramic cylinder is more desirable. However, three shorter cylinders had to be used since the holes in the cylinders can not be machined with close tolerances for lengths greater than about 2 inches. Ferrite rod lengths are also constrained by the machining process, and only rod lengths less than 10 inches are available. The tolerance limit for the diameters of the ferrite rod and ceramic cylinders is about ± 0.1 mil (100 microinches), which dictates the minimum obtainable air gaps using a machining process.

The design equations in Section 4.1 were used to determine the design parameters (Figure 4) such as the diameters and the helix turns per inch. By assuming no air gaps in the line, approximately 2.5 nanosecond/cm time delay variability is possible based on calculations. With a 1.0 mil air gap, a time delay variability of 1.25 nanoseconds/cm is possible, again based on calculations. As will be seen in the next section, about 0.75 nanosecond/cm was actually measured. This result indicates the air gaps in the constructed line were greater than 1 mil. Clearly, the precision of the line construction significantly affects the obtainable time delay variability.

4.4 EXPERIMENTAL RESULTS FOR HF DELAY LINE

Descriptions of the test instrumentation and procedures used to make the experimental measurements are in Appendix B. Results for both design models are presented starting with Design Model 1.

4.4.1 DESIGN MODEL 1

Measured characteristics as a function of frequency are shown in Figure 6. The group delay was measured for three different levels of applied dc magnetic field. Also shown on the graph is the insertion loss at the same three magnetic field levels. Notice that both the group delay and insertion loss decrease as the applied dc magnetic field increases. Another set of characteristics were measured as a function of the applied dc magnetic field with the frequency held constant. These results are shown in Figure 7, 8, 9, 10, 11, and 12 for frequencies of 4 MHz, 8 MHz, 16 MHz, 30 MHz, 50 MHz, and 100 MHz, respectively. Both group delay and phase delay (see Appendix A) measurements are displayed. Notice that the phase delay has been normalized while the group delay points are the absolute values. Figure 13 is a graph of the measured input impedance as a function of frequency and applied dc magnetic field.

Table I lists the results of intermodulation measurements made on Design Model 1. Both input signals (f_1 and f_2) were at 2 watts average power. The intermodulation levels are the maximum levels observed while varying the applied dc magnetic field.

The power-handling capability of Design Model 1 was tested by applying 50 watts average power for a 3-hour period. The model is capable

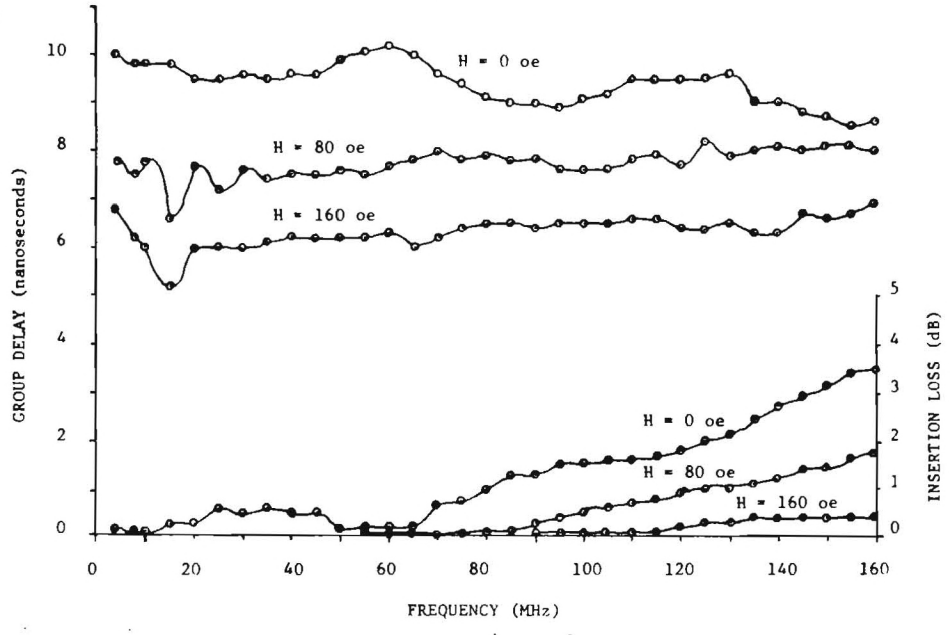

Figure 6. Characteristics of the Ferrite-Loaded Helical Line Design Model 1 at Different Applied DC Magnetic Field (H) Levels

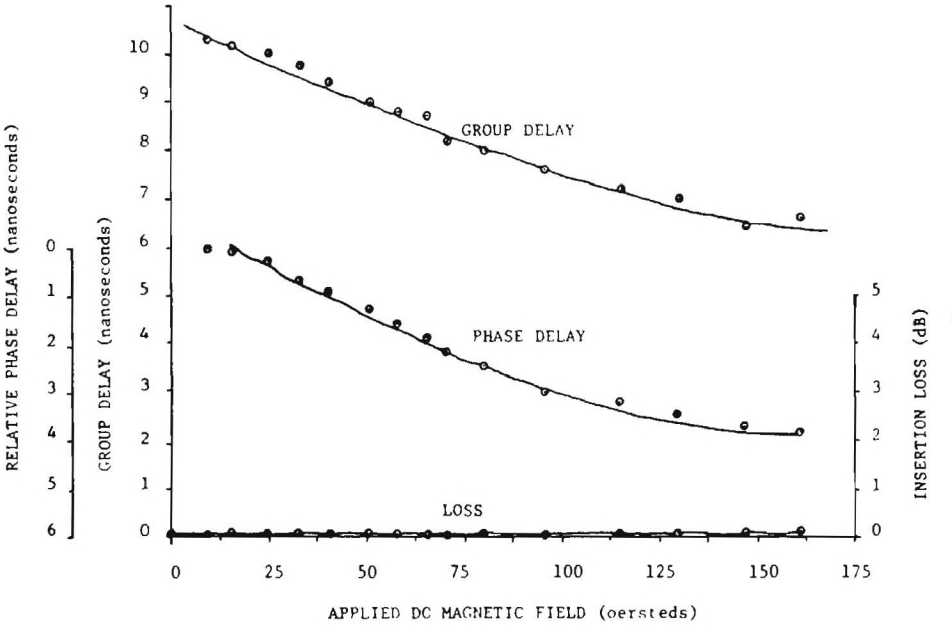

Figure 7. Characteristics of the Ferrite-Loaded Helical Line Design Model 1 at 4 MHz

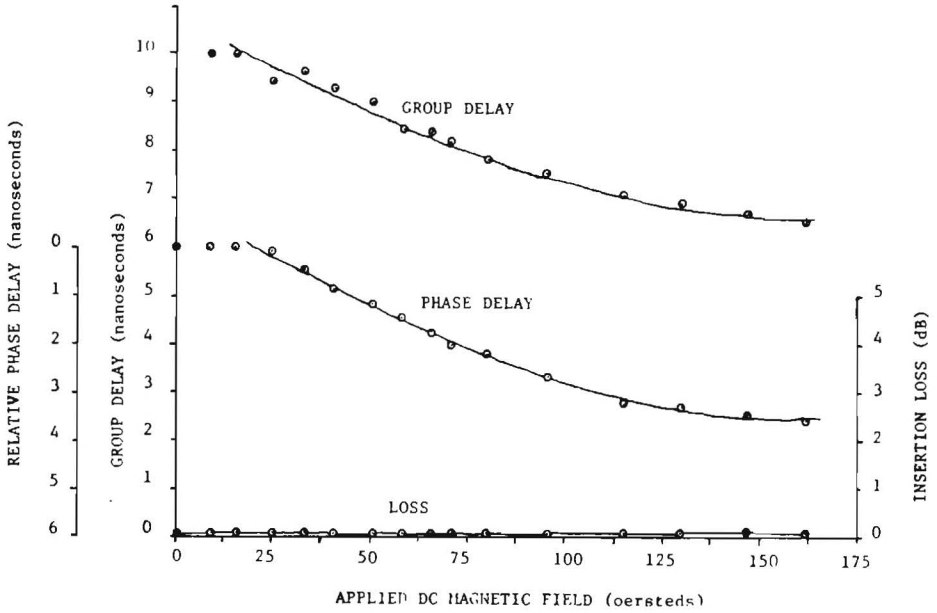

Figure 8. Characteristics of the Ferrite-Loaded Helical Line Design Model 1 at 8 MHz

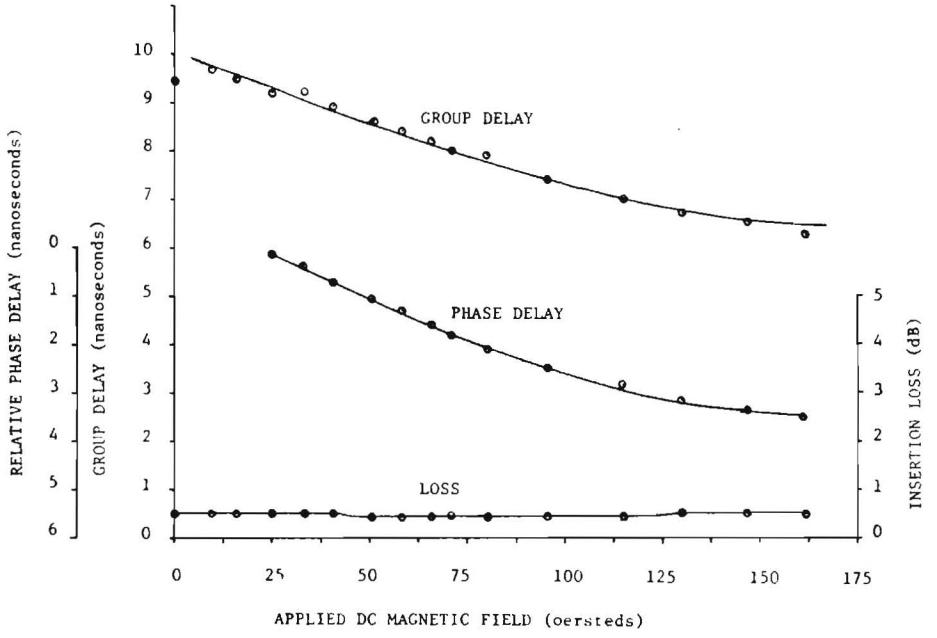

Figure 9. Characteristics of the Ferrite-Loaded Helical Line Design Model 1 at 16 MHz

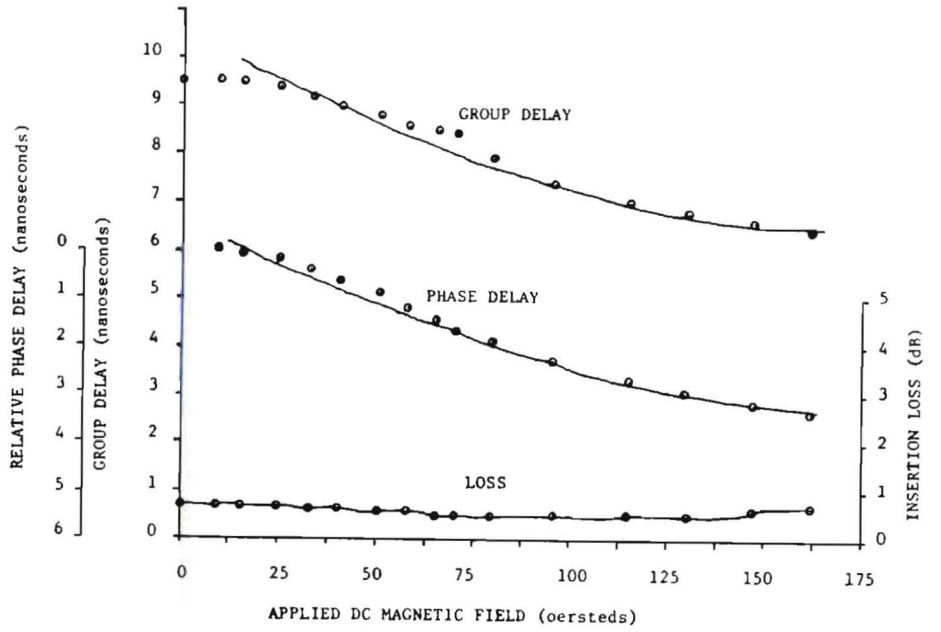

Figure 10. Characteristics of the Ferrite-Loaded Helical Line Design Model 1 at 30 MHz

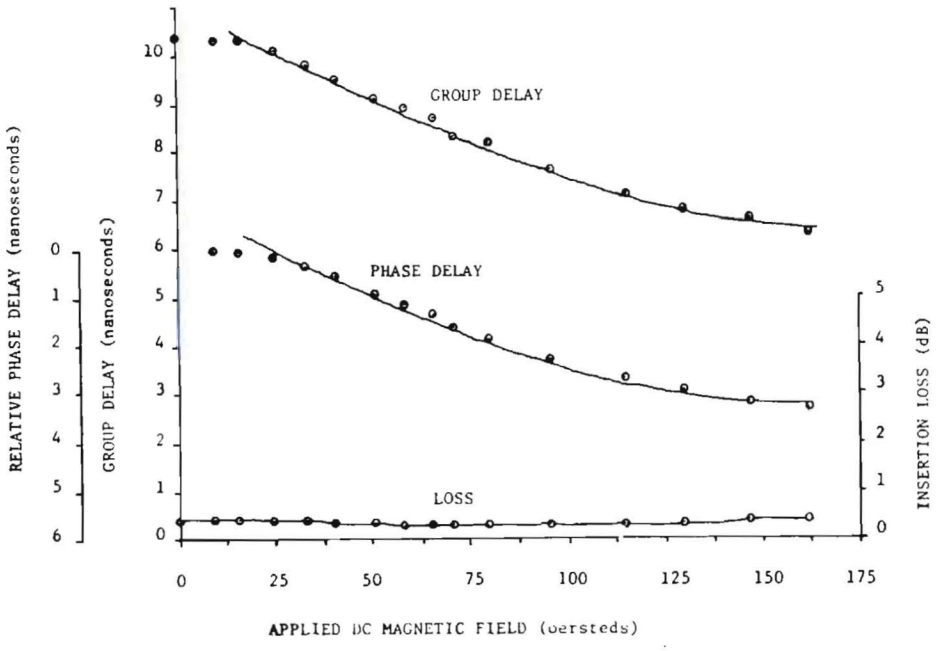

Figure 11. Characteristics of the Ferrite-Loaded Helical Line Design Model 1 at 50 MHz

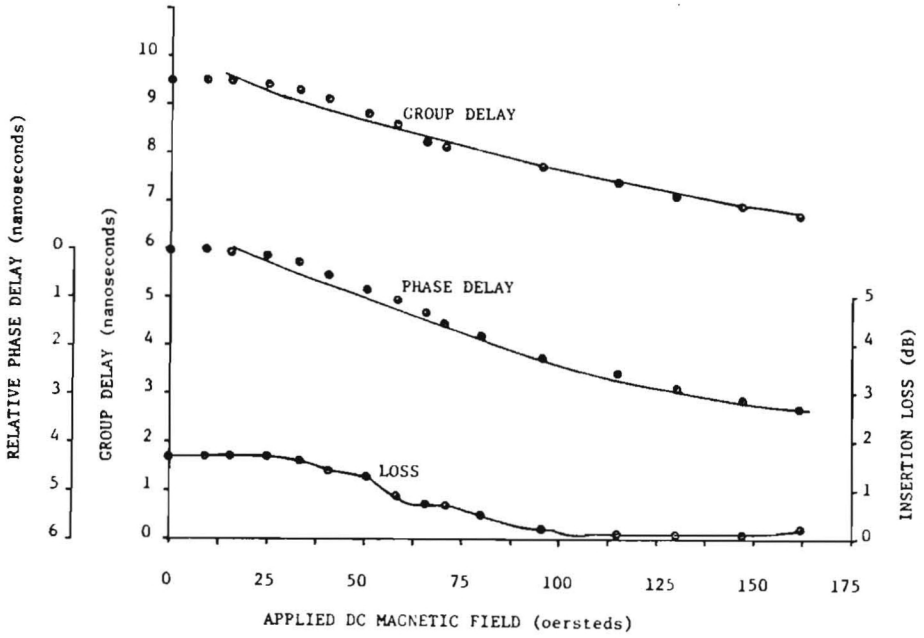

Figure 12. Characteristics of the Ferrite-Loaded Helical Line Design Model 1 at 100 MHz

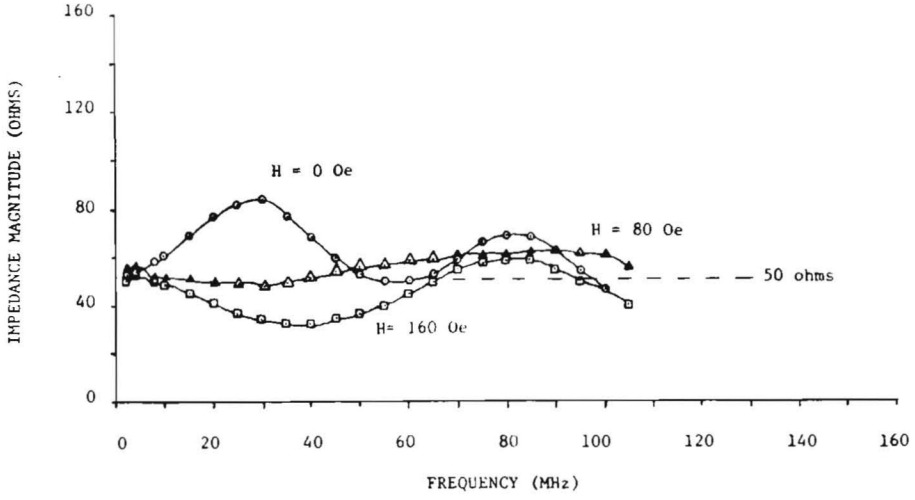

Figure 13. Impedance of the Ferrite-Loaded Helical Line Design Model 1 at Different Applied DC Magnetic Field (H) Levels

TABLE I

INTERMODULATION PRODUCTS LEVELS FOR DESIGN MODEL 1

TEST FREQUENCIES	IM PRODUCT LEVELS
f_1 = 30 MHz, 2 watts	5MHz, -60 dB
f_2 = 35 MHz, 2 watts	60 MHz, -60 dB
	65 MHz, -53 dB
	70 MHz, -58 dB
f_1 = 25 MHz, 2 watts	5 MHz, -62 dB
f_2 = 30 MHz, 2 watts	50 MHz, -62 dB
	55 MHz, -58 dB
	60 MHz, -60 dB
f_1 = 25 MHz, 2 watts	10 MHz, -60 db
f_2 = 35 MHz, 2 watts	50 MHz, -58 dB
	60 MHz, -54 dB
	70 MHz, -58 dB

of 50 watts, and during the test period, no variation in the insertion loss was observed.

4.4.2 DESIGN MODEL 2

The basic measurements made on Design Model 1 were also made for Design Model 2. Figure 14 shows the characteristics of Design Model 2 as a function of frequency and applied dc magnetic field. The measured group delay of Design Model 2 is not as flat as the group delay for Design Model 1. This increased variation in group delay occurred because the characteristic impedance of Design Model 1 is much greater than 50 ohms. Figure 15 shows the measured input impedance. Notice that the peaks and troughs of the group delay data are related to the input impedance variations.

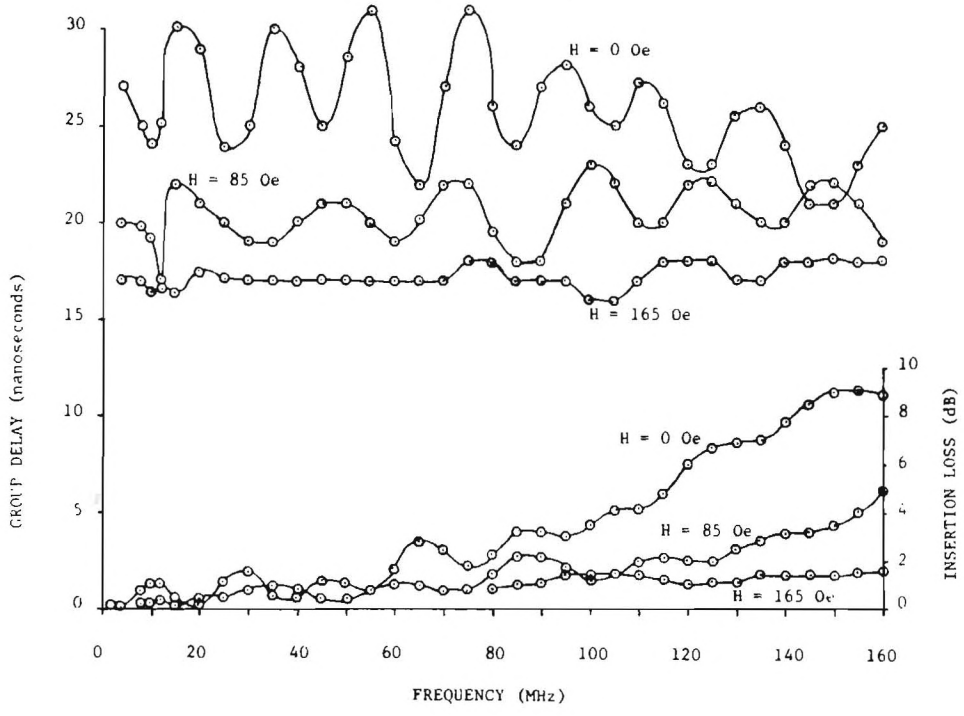

Figure 14. Characteristics of the Ferrite-Loaded Line Design Model 2 at Different Applied DC Magnetic Field (H) Levels

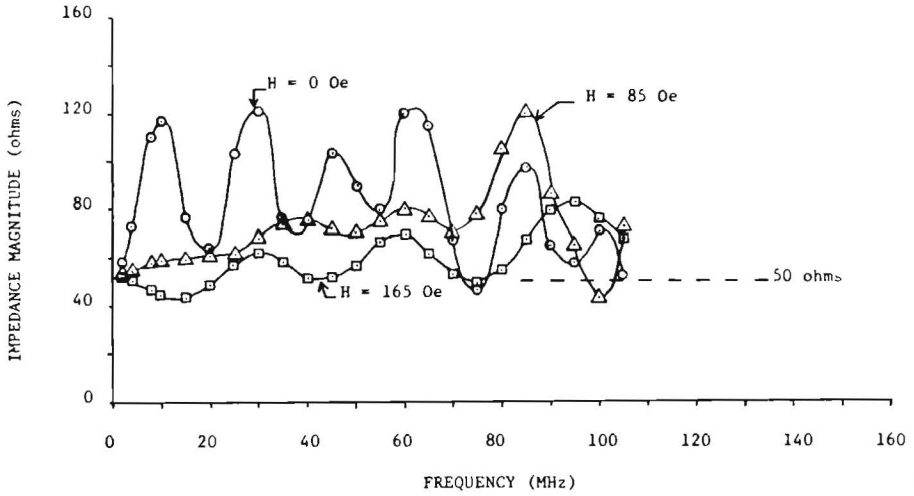

Figure 15. Input Impedance of the Ferrite-Loaded Helical Line Design Model 2 at Different Applied DC Magnetic Field (H) Levels

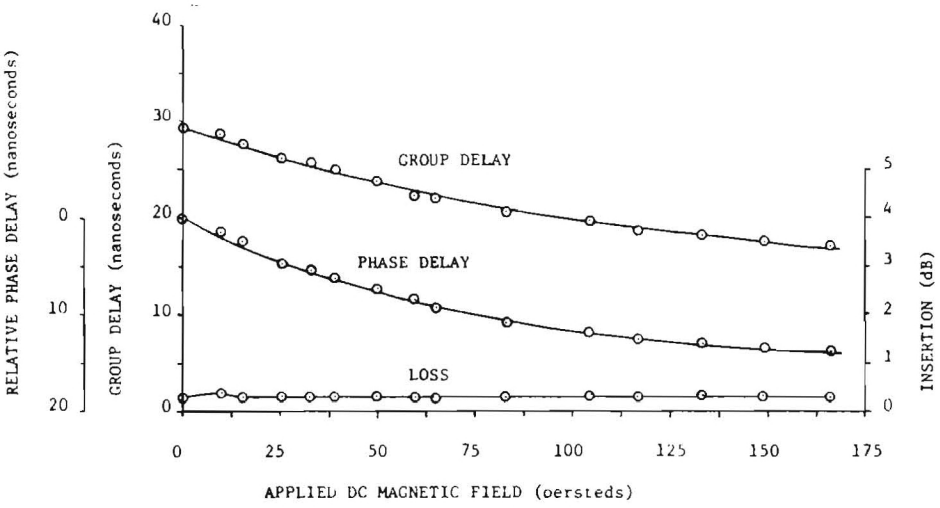

Figure 16. Characteristics of the Ferrite-Loaded Helical Line Design Model 2 at 2 MHz

The group delay variations of Design Model 2 can likely be reduced considerably through redesign. The characteristics of Design Model 2 as a function of applied dc magnetic field with frequency fixed are shown in Figures 16, 17, 18, 19, 20, and 21 for 2 MHz, 4 MHz, 8 MHz, 16 MHz, 30 MHz, and 50 MHz, respectively.

Intermodulation measurements for Design Model 2 are listed in Table II. A comparison with the Design Model 1 intermodulation products reveals that Design Model 2's are at higher level. The reason for this increase is not completely understood, but may be caused by the higher VSWR levels in Design Model 2 or may result from the permeability rate of change due to the differences in lengths.

The power-handling capability of Design Model 2 was tested in the same manner as for Model 1. Again the model can handle the 50 watts, and no variation in the insertion loss was observed.

4.5 CONCLUSIONS - HF DELAY LINE RESULTS

The design principles, method of construction, and experimental results for the HF variable delay line have been investigated. The use of the ferrite-loaded helical line to meet the design objectives has been shown to be a viable technique. The insertion loss and frequency range objectives were exceeded. For example, the line is capable of operating up to 80 MHz. The 10-nanosecond time delay variability can be met using a line that is approximately 6.0 inches long. Since the line is electrically controlled, the time delay variation rate of 15-20 Hz can be easily obtained. The time delay variation is continuous with the applied dc magnetic field and small time delay resolution is obtainable. The line can handle 50 watts average power. The intermodulation measurements showed the line had good linearity, and the linearity may possibly be improved further through improved construction techniques or through use of different materials.

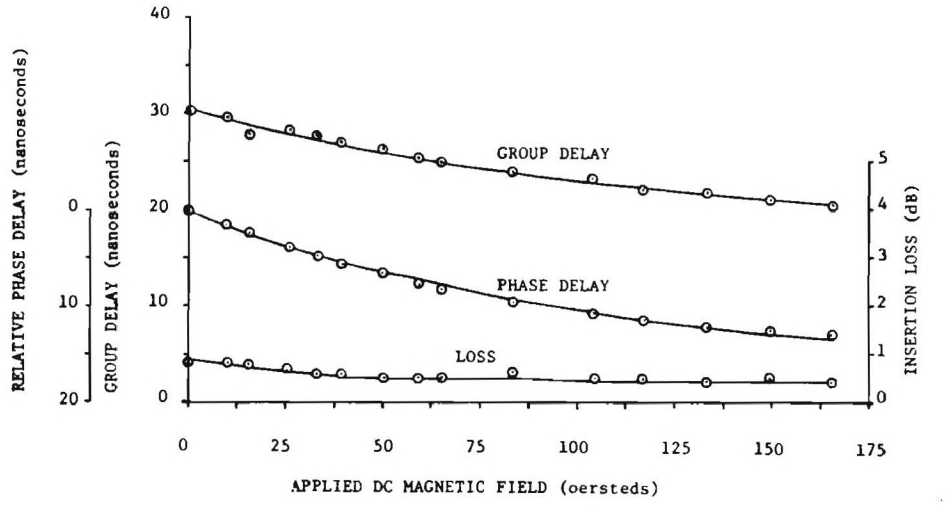

Figure 17. Characteristics of the Ferrite-Loaded Helical Line Design Model 2 at 4 MHz

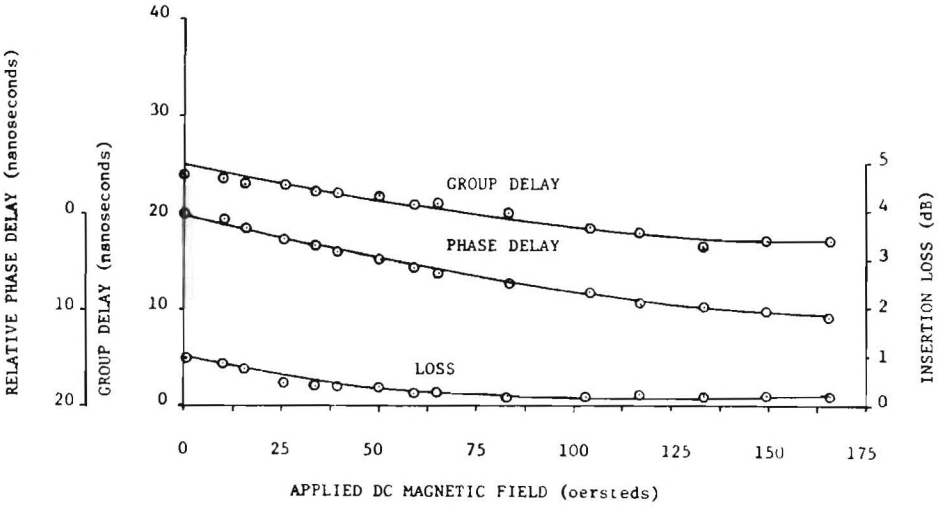

Figure 18. Characteristics of the Ferrite-Loaded Helical Line Design Model 2 at 8 MHz

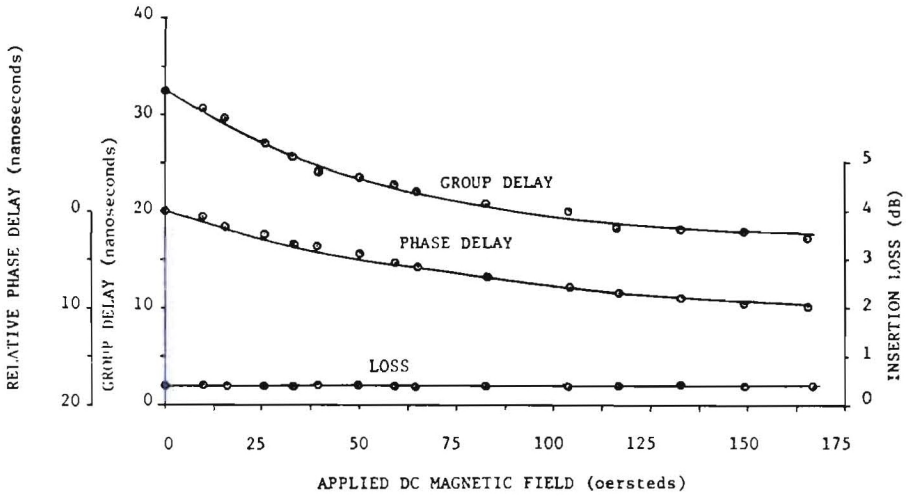

Figure 19. Characteristics of the Ferrite-Loaded Helical Line Design Model 2 at 16 MHz

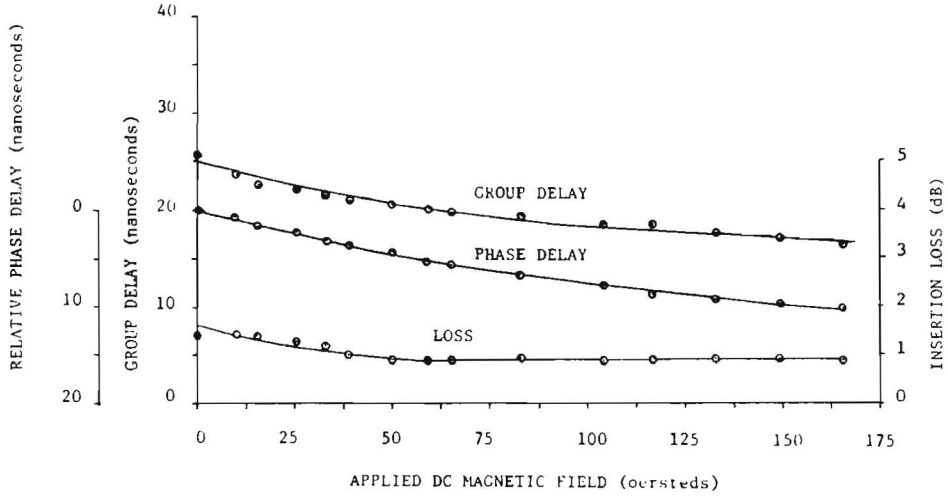

Figure 20. Characteristics of the Ferrite-Loaded Helical Line Design Model 2 at 30 MHz

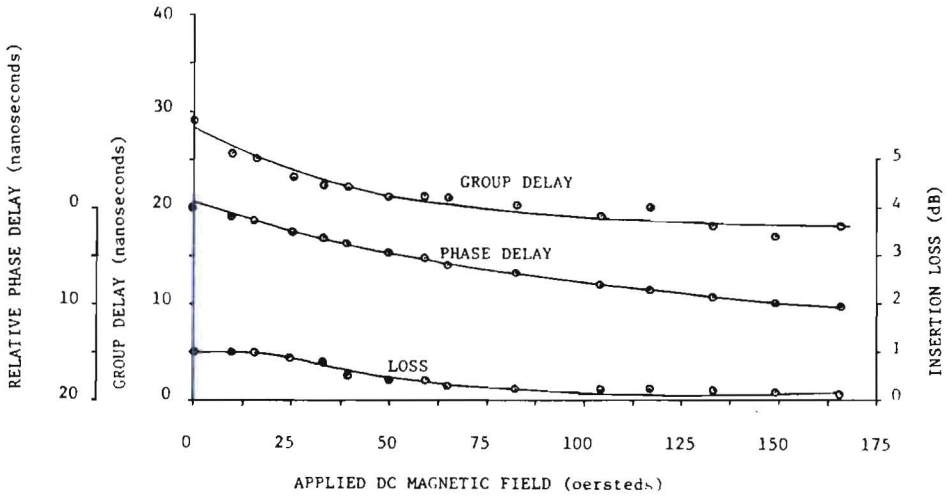

Figure 21. Characteristics of the Ferrite-Loaded Helical Line Design Model 2 at 50 MHz

TABLE II

INTERMODULATION PRODUCTS LEVELS FOR DESIGN MODEL 2

TEST FREQUENCIES	IM PRODUCT LEVELS
f_1 = 30 MHz, 2 watts	5 MHz, -62 dB
f_2 = 35 MHz, 2 watts	60 MHz, -52 dB
	65 MHz, -46 dB
	70 MHz, -54 dB
f_1 = 25 MHz, 2 watts	5 MHz, -60 dB
f_2 = 30 MHz, 2 watts	50 MHz, -56 dB
	55 MHz, -50 dB
	60 MHz, -54 dB
f_1 = 25 MHz, 2 watts	10 MHz, -56 dB
f_2 = 35 MHz, 2 watts	50 MHz, -56 dB
	60 MHz, -50 dB
	70 MHz, -54 dB

5.0 UHF VARIABLE DELAY LINE

A version of the ferrite-loaded helical line was considered for the UHF delay line. However, early in the program, based on the trade-offs discussed in Section 4.2, preliminary designs showed that the ferrite-loaded helical line would be very lossy and would probably exceed the design objective of 7 dB. Based on this conclusion and consideration of alternatives, it was determined that the coupled helical transmission line had promise as a viable UHF variable time delay technique. This is the technique reported on in this section.

5.1 UHF DELAY LINE DESIGN PRINCIPLES

A number of investigators [6-10] has studied the coupled helical transmission line. The design principles discussed here are based on these earlier studies. Figure 22 shows a simplified coupled helical line. The axial phase velocity on the open helix is a fraction of the free-space phase velocity. By mechanically changing the position of the movable coupler, the time delay is varied. There is no electrical contact between the couplers and the open helix. A few inches of separation between the fixed coupler and the movable coupler can be equivalent to a few feet of separation in free space.

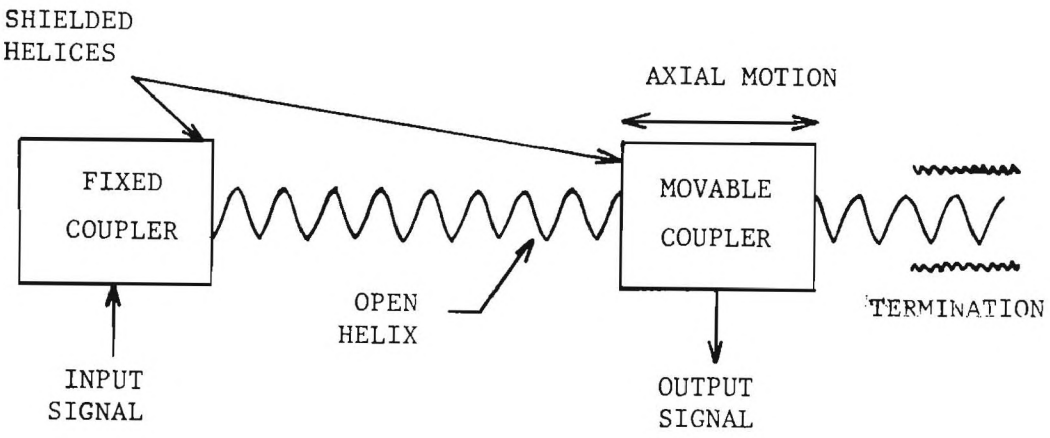

Figure 22. Simplified Coupled Helical Line

The property of an open helical transmission line that makes it useful for time delay applications is that, over a wide frequency range, a current wave travels at approximately the velocity of light along the helical conductor, and when the wave is observed from the axial direction, a relative retardation results. The relative retardation is equal to the ratio of the circumference of a helix turn to the helix pitch. This ratio is defined as the delay factor and is equal to:

$$\text{Delay factor} = \frac{\text{wave velocity along conductor}}{\text{wave velocity along axis}} \tag{9}$$

$$= \frac{c}{v_p} = \frac{h}{k}$$

where

c = velocity of light

v_p = velocity in axial direction

k = free-space propagation constant

h = axial propagation constant.

The delay factor is also equal to:

$$\text{Delay factor} = \frac{\text{length of helix turn}}{\text{pitch}} . \tag{10}$$

The pitch angle is defined as:

$$\psi = \tan^{-1} \frac{p}{2\pi a} \tag{11}$$

where

p = pitch in inches

a = helix turn radius in inches.

The length of a helix turn is equal to $p \csc\psi$. Substituting this relationship in Equation 10 gives:

$$\text{Delay factor} = \csc\psi. \tag{12}$$

From the above equations, it is evident that the helix velocity ratio can be adjusted by changing the helix diameter and the pitch. The propagation characteristic of an open helix is shown in Figure 23. There are certain regions that are excluded for slow wave propagation. If the open helical line is operated in the excluded regions, it becomes an inefficient transmission line and power radiates from the line. The mode characteristics of interest are labeled "1" in the Figure 23. This method of operation is referred to as the slow wave or delay-line mode of propagation.

A shielded helix is also needed to construct the coupled helical line. The shielded helix is a concentric helix within a conducting cylinder. The shielded helix propagation characteristics are similar to the open helix except that modes can now exist in the excluded regions of propagation. These modes have cutoff frequencies and propagation characteristics similar to those that can exist in cylindrical waveguides. The conducting cylinder of the shielded helix does affect the propagation characteristics. However, to a first approximation the shielded helix dimensions can be selected using the equations for the open helical line.

Next consider the coupling between two helices where an open helix is concentrically placed inside the shielded helix. This configuration is the coupling method used for the coupled helical line. According to Kompfner's investigations and studies [8] if the helices are oppositely

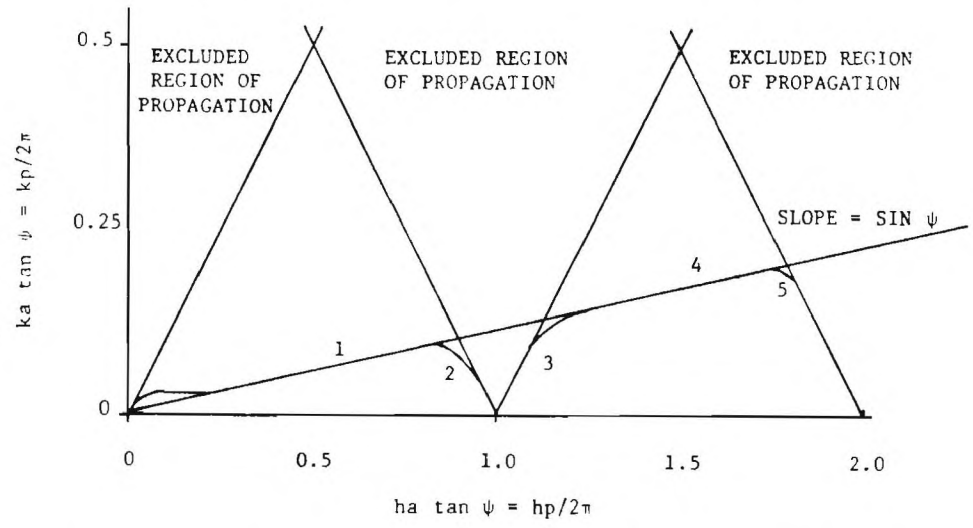

Figure 23. Propagation Characteristics for Helical Line.

wound and the phase velocities on each helix are equal, complete unidirectional power transfer takes place when the helices are coupled over a length. Kompfner also showed that the beat wavelength between the two helices is stationary with respect to frequency, if the correct choice of geometrical parameters is made. To obtain stationary beat wavelength, the radius of the shielded helix should be approximately 1.5 times that of the open helix. The beat frequency is the rate at which power is transferred from one helix to the other and back when the two helices have equal phase velocities. The beat wavelength is equal to [8]:

$$\lambda_c = 2\pi e(b-a) \tag{13}$$

where

e = 2.718

b = shielded helix radius in inches

a = open helix radius in inches.

The shielded helix length should be approximately equal to one-quarter beat wavelength for maximum power transfer to the open helix. The number of turns for the shielded helix is equal to the one-quarter beat wavelength divided by the helix pitch.

The input impedance of the shielded helix is a function of the shield and helix diameters, the helix pitch, and the dielectric material between the helix and shield. Kirschbaum [11] presents equations and graphs for the characteristic impedance of the shielded helix.

Calculations by Peters [12] predict that for minimum attenuation and peak power-handling capability the ratio of the helix wire diameter to the helix pitch should be approximately equal to 0.35. The power-handling capability of the coupled helical line is limited by the breakdown voltage between the shielded helix shield and its helix. Since the breakdown voltage of air is 75 peak volts/mil, the coupled helical line can be readily designed for 50 watts. In fact, Stark [7] designed a coupled helical line that had 350 kW power-handling capabilities.

The frequency range of the coupled helical line is limited for a given set of geometrical parameters. As the frequency increases, a point is reached

where the helix circumference is greater than a half free-space wavelength. Above this frequency, high order modes occur and the coupled helical becomes inefficient. As the frequency decreases, the ratio of the helix wave velocity along the conductor becomes approximately equal to the axial wave velocity, and a delay factor of unity results. The diameters of the helicies can be made larger to increase the delay factor, but the physical dimensions of the coupled helical line become unwieldy.

5.2 UHF LINE MODEL CONSTRUCTION

The coupled helical line was designed using the design principles discussed previously. A delay factor of 9.5 was initially selected, and the geometric dimensions were calculated using the design equations. Figure 24 shows the coupled helical line configurations and its design data. A picture of the line is shown in Figure 25. Notice this is a double coupled helical line. This configuration has twice the time delay variation as compared to the single helical line. The configuration also has the advantage that the input and output cables remain fixed.

After the coupled helical line was constructed, the pitch of the open helix was adjusted to minimize the coupling variation as a function of frequency. Even after these adjustments, it was found that terminations were necessary on each end of the open helical lines to reduce reflections. These terminations were constructed from Du Pont P 60703 resistive paper. Two triangles 6 inches in height with 2.25-inch bases were cut from the resistive paper. The triangles were wrapped around the inside circumference of the open helix. The apex of the triangles pointed along the axial direction of open helix. By terminating the shielded helix in a 330-ohm resistor, reflections were further reduced.

5.3 EXPERIMENTAL RESULTS FOR UHF DELAY LINE

The test instrumentation and procedures used to make the experimental measurements are found in Appendix B. Time delay, insertion loss, and VSWR characteristics were measured.

The measured group delay as a function of frequency for different coupler separation distances is shown in Figure 26. The separation is the distance L_5 in Figure 24. Positioning the movable coupler from 2.0 inches to 16.0 inches results in an average group delay variation of 15 nanoseconds.

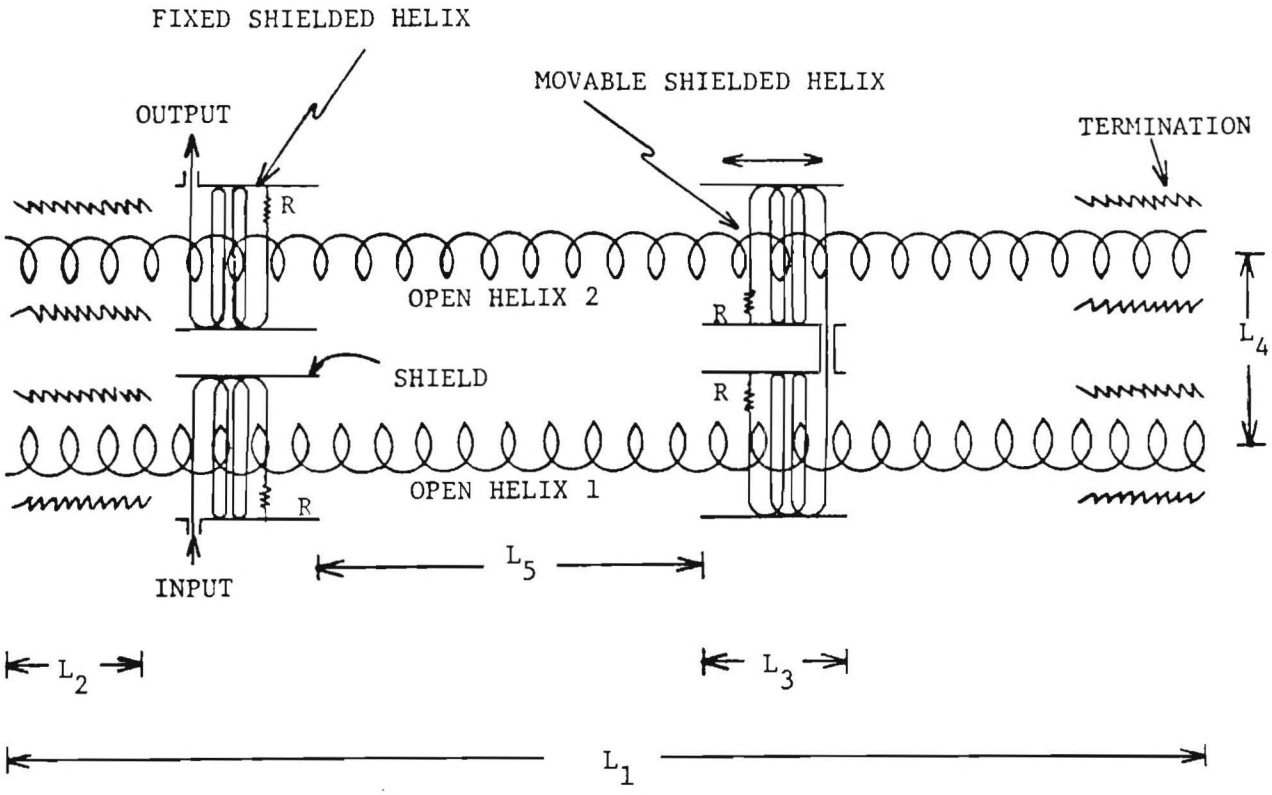

HELICAL LINE DESIGN DATA

Open helix form	1.5" OD x .125" wall polystyrene
Shielded helix form	2.25" OD x .125" wall polystyrene
Open helix	.125" OD copper tubing, .625" pitch, 1.6 tpi
Shielded helix	.25" OD copper tubing, .88" pitch, 1.13 tpi
Shield	2.875" ID x 2.0" length copper tubing
Open helix length	29.5 inches (L_1)
Open helices separation	5.5 inches (L_4)
Open helix termination	6.0 inches (L_2), resistive paper (du Pont P60703)
Shielded helix load	330 ohm resistor (R)

Figure 24. Coupled Helical Line Configuration and Design Data

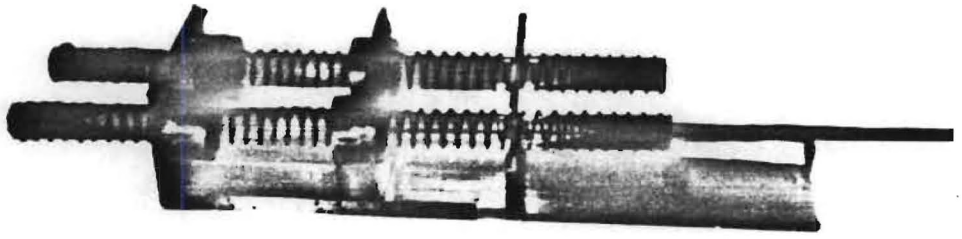

Figure 25. Photograph of Coupled Helix

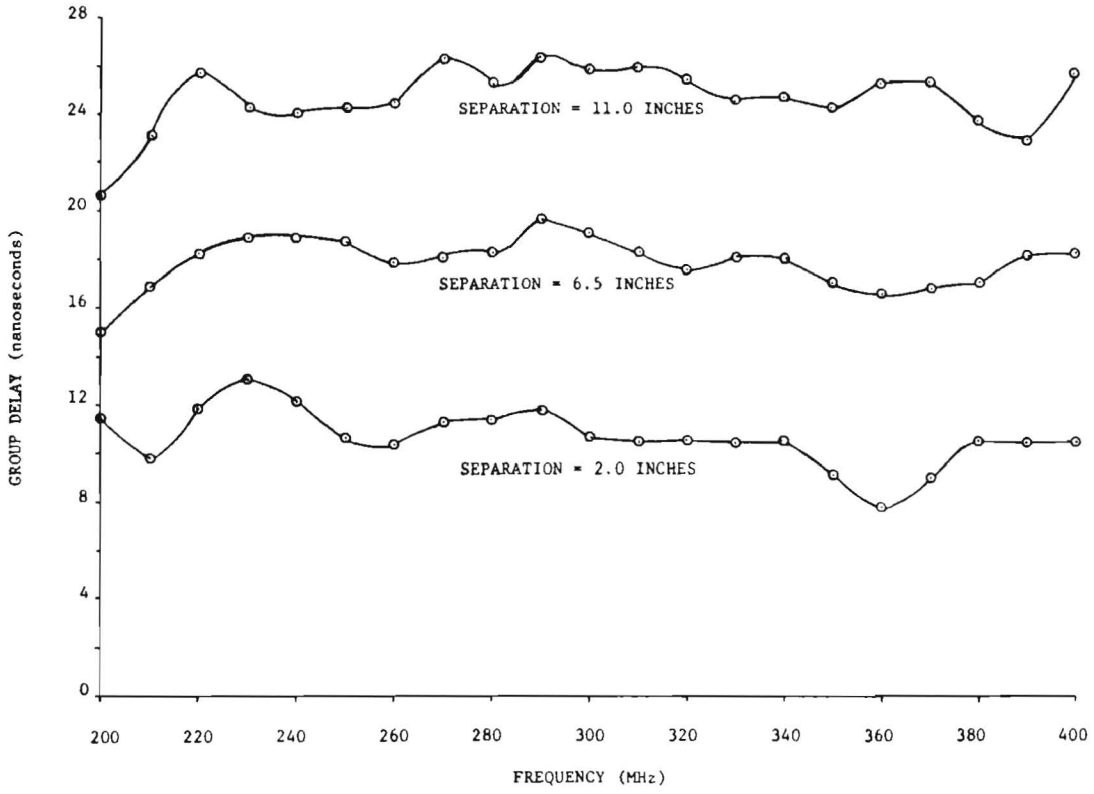

Figure 26. Time Delay of the Coupled Helical Line at Different Coupler Separations.

The variation of the group delay is attributed to reflections. The presence of reflections is evident in Figure 27, which shows the VSWR of the coupled helical line at the same coupler separations.

The time delay characteristics as a function of coupler separation for frequencies 200 MHz, 300 MHz, and 400 MHz are graphed in Figures 28, 29, and 30, respectively. Both the group and phase delay (see Appendix A) are plotted. Considerable variations, particularly in Figure 28, are evident in the group delay, and these variations are again attributed to reflections.

The measured insertion loss is given in Figure 31. Insertion loss varied from 9 to 14 dB which is somewhat higher than the 7 dB design objective. Measurements showed that most of the loss occurs in the couplers.

Power-handling capability of the coupled helical line was not tested. Other investigators [7] have shown the line can be designed for kilowatt power levels.

Measurements of the time delay resolution were made. Resolution of ±0.1 nanoseconds were observed, but measurements to the accuracy of ±0.01 nanosecond were beyond the instrumentation resolution capability.

5.4 CONCLUSIONS - UHF DELAY LINE RESULTS

A coupled helical line has been investigated as a candidate technique to meet the UHF delay line design objectives. The design principles have been outlined, a model has been constructed, and experimental measurements have been completed. Time delay characteristics, insertion loss, and VSWR were measured.

The line can meet the time delay variation objective of 10 nanoseconds and the frequency range objective of 200-400 MHz. Even though the power-handling capability was not tested, the design of the line makes it inherently capable of high-power levels.

The insertion loss varied from 9-14 dB and is somewhat above the design objective of 7 dB. Reflections are a problem on the line. However, it is felt that the insertion loss and the reflections can be reduced by improving the couplers and terminations through redesign.

The coupled helical line is mechanically controlled. Measurements showed that time delay resolution was at least ±0.1 nanosecond. The time delay resolution and variation rate will depend on the mechanical positioner design.

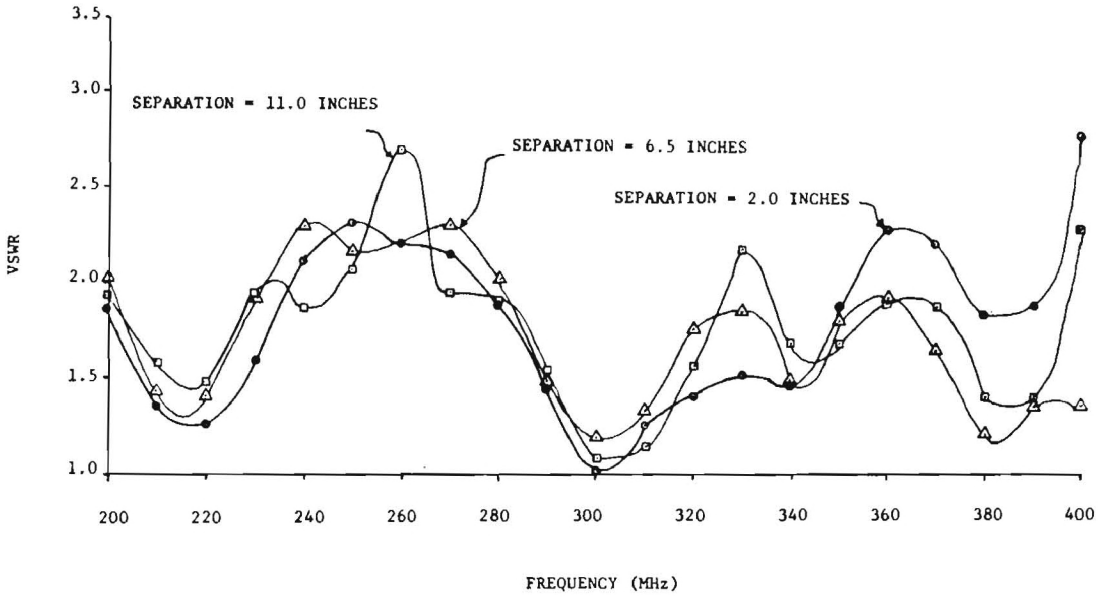

Figure 27. VSWR of the Coupled Helical Line at Different Coupler Separations

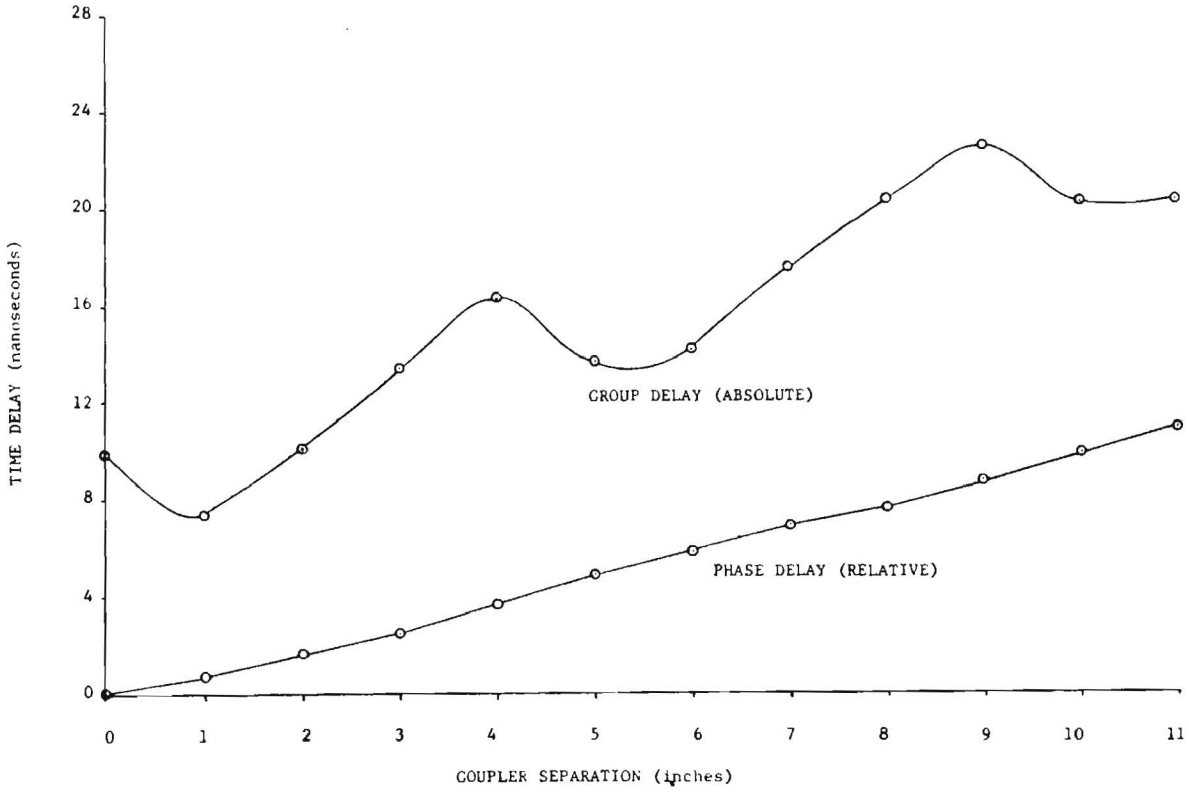

Figure 28. Time Delay Characteristics at 200 MHz of the Coupled Helical Line

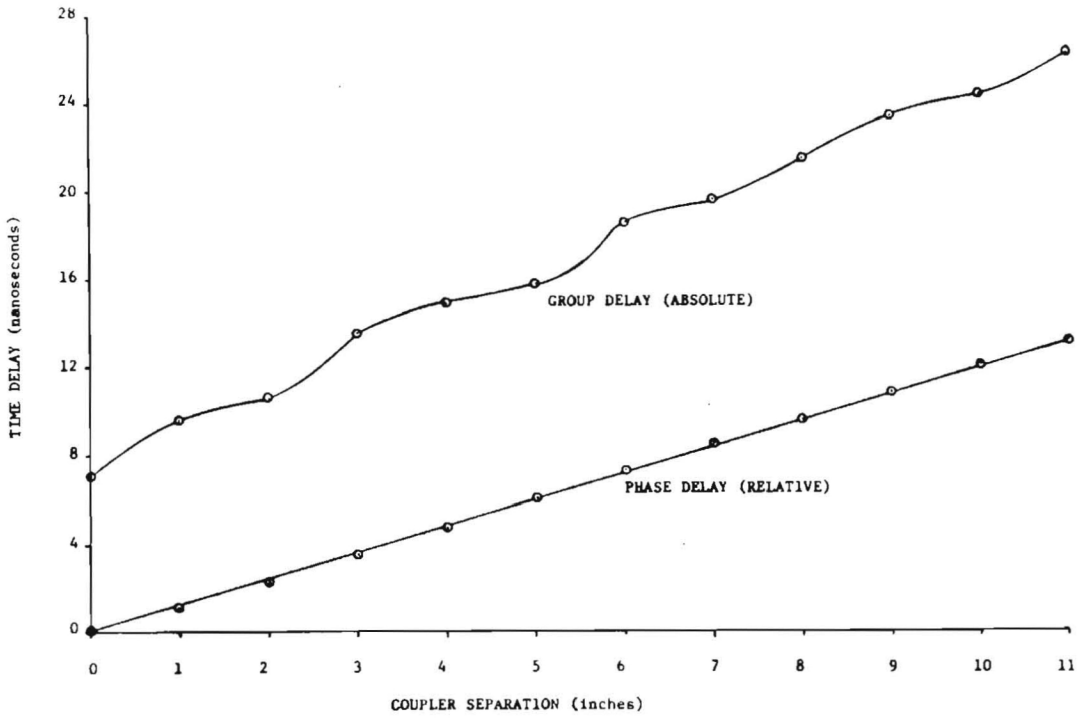

Figure 29. Time Delay Characteristics at 300 MHz of the Coupled Helical Line

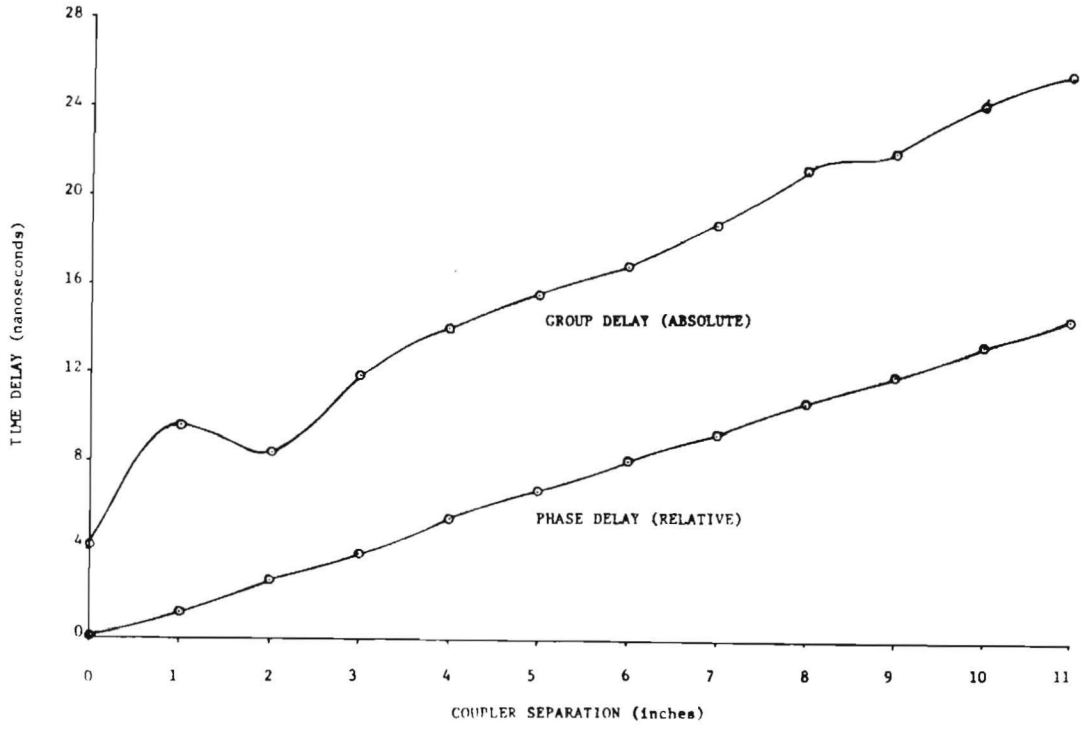

Figure 30. Time Delay Characteristics at 400 MHz of the Coupled Helical Line

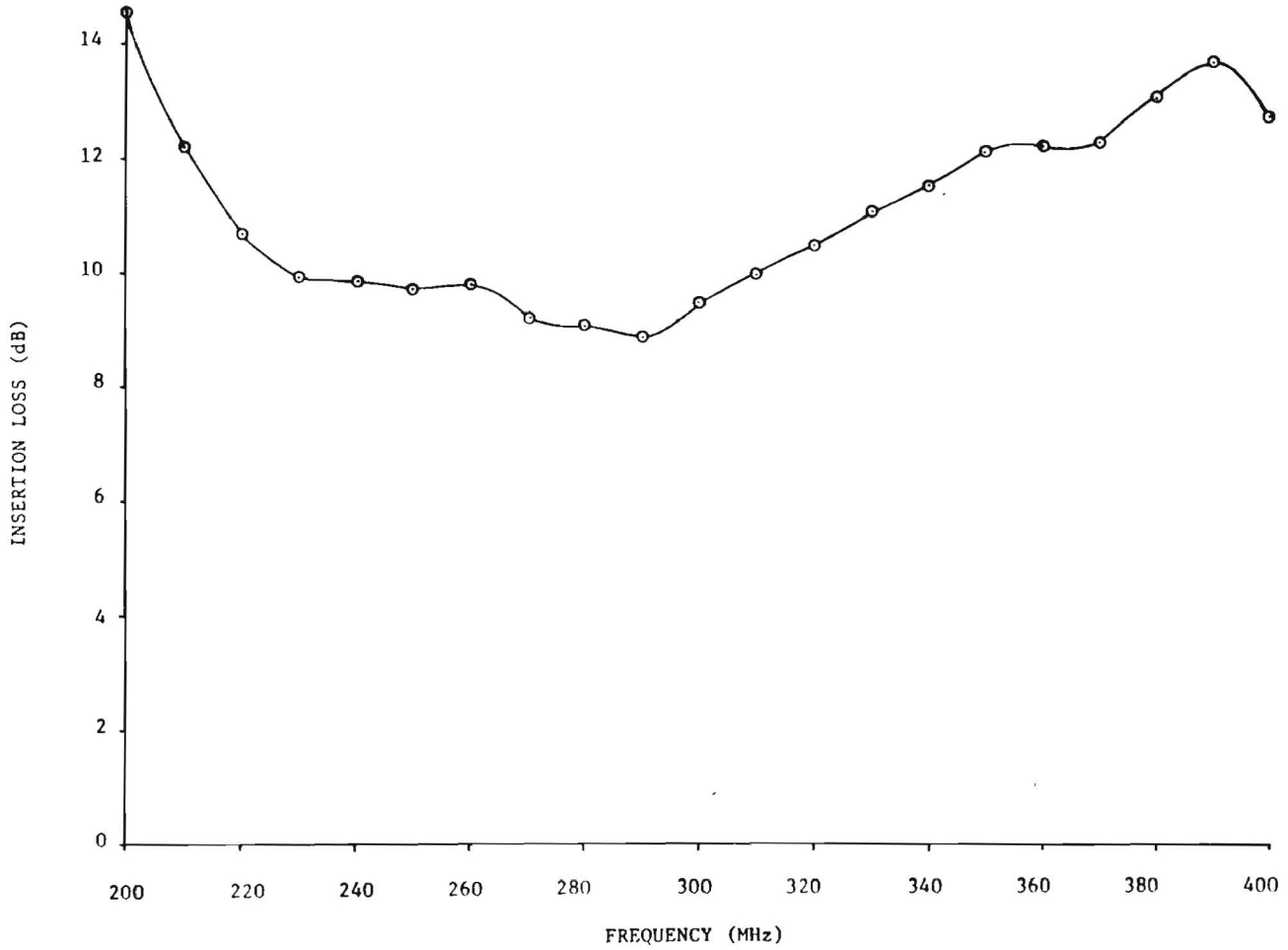

Figure 31. Insertion Loss of the Coupled Helical Line for Coupler Separation = 11.0 inches

6.0 SUMMARY AND RECOMMENDATIONS

Two techniques have been identified as viable candidates to fulfill the design objectives for an HF and UHF variable time delay line. For the HF line, a ferrite-loaded helical line, that is electrically controllable, has been designed, constructed, and tested. For the UHF line, a coupled helical transmission line, that is mechanically controllable, has also been designed, constructed, and tested.

Experimental results for the ferrite-loaded helical line were very good. Based on the results, most of the design objectives can be met with this line. However, further improvements may be possible with more precise construction. Design models with different ferrite compositions or larger diameter (increased volume per unit length) ferrite rods may improve linearity further and thus improve the intermodulation product levels. By machining a helix form into the ferrite rod and metallizing over the form, a more precise construction will result and thus reduce the thickness of air gaps. This construction would be expected to improve the time delay variability per unit length. As a recommendation, consideration should be given to using strontium titanate in place of calcium titanate. Strontium titanate has a dielectric constant of 250 as compared to 140 for the calcium titanate. The higher dielectric constant will improve even further the time delay variability per unit length.

Experimental results for the coupled helical line were encouraging. Improvements are recommended to meet all the design objectives. Reflections cause group delay ripple. However, it is felt that the reflections can be reduced through improved or different coupler designs and through improved terminations. Further research is needed to define the obtainable time delay resolution and time delay variation rate using different mechanical positioners.

7.0 REFERENCES

1. Clark, D. E. and W. R. Hardell, "Adaptive Time Delay Circuitry for Interference Cancellation Systems", Final Technical Report, RADC-TR-80-114, April 1980, (AD A086 326).

2. Megla, G. K., L. C. Gunderson, and J. Singletary, "A Low-Impedance Helical Delay Line", Microwave Journal, January 1968,pp. 55-59.

3. Reference Data for Radio Engineers, ITT Corporatrion, Fourth Edition, p. 595.

4. Sakiotis, N. G. and D. E. Allen, "UHF Phase Shifter", Final Report, AFCRL 391, March 15,1961, (AD 262 711).

5. Pippin, J. E. and C. L. Hogan, "Initial Permeability Spectra in Ferrites and Garnets", Scientific Report No. 1., April 1, 1959, (AD 214 412).

6. Sensiper, Samuel, "Electromagnetic Wave Propagation on Helical Conductors", Technical Report 194, Massachusetts Institute of Technology, Research Laboratory of Electronics, May 16, 1951.

7. Stark, Louis, "A Helical-Line Phase Shifter for Ultra-High Frequencies", Technical Report 59, Massachusetts Institute of Technology, Lincoln Laboratory, February 4, 1954.

8. Kompfner, R., J. S. Cook and C. F. Quate, "Coupled Helices", The Bell System Technical Journal, January 1956, pp. 127-178.

9. Crandell, Paul A. and Frederick J. Dominick, "A Helical Phase Shifter for VHF", Microwave Journal, September/October 1958, pp. 29-32.

10. Okvbo, George H., "Helix Frequency Scanning Feed", Microwave Journal, December 1965, pp. 39-44.

11. Kirschbaum, Herbert S., "The Characteristic Impedance and Phase Velocity of a Shielded Helical Transmission Line", Carnegie Institute of Technology Thesis, June 1953.

12. Peters, R. W., J. A. Rultz and A. B. Olson, "Attenuation of Wire Helices in Dielectric Supports", RCA Review, December, 1952, pp. 558-572.

APPENDIX A

TIME DELAY RELATIONSHIPS

Ideally, the signal through a delay line should propagate without any distortion (variation) in phase or amplitude. Such characteristics are especially desirable for a delay line used in an ICS. Figure A-1(a) shows the ideal characteristics for a distortionless (but lossy) transmission line. The loss is constant and the phase is linear within the bandwidth of interest. Of course for a distortionless and lossless transmission line $\alpha \ell = 0$.

The phase delay is defined as the slope of the $\beta\ell$ curve in Figure A-1(a). Thus phase delay is equal to:

$$t_p = \frac{\beta_o \ell}{\omega_o} \tag{A-1}$$

where

t_p = phase delay in seconds
β_o = phase constant in radians/second
ω_o = radian frequency ($2\pi f$)
ℓ = length of delay line in meters.

The phase velocity is equal to:

$$v_p = \frac{\omega}{\beta} \text{ meters/second.} \tag{A-2}$$

Substituting Equation A-2 into A-1 gives:

$$t_p = \frac{\beta_o \ell}{\omega_o} = \frac{\ell}{v_p} \quad . \tag{A-3}$$

The phase velocity is the rate at which a single-frequency sinusoid wave moves down a line and, for an ideal line, it is the velocity of propagation. The phase velocity is sometimes called the carrier velocity.

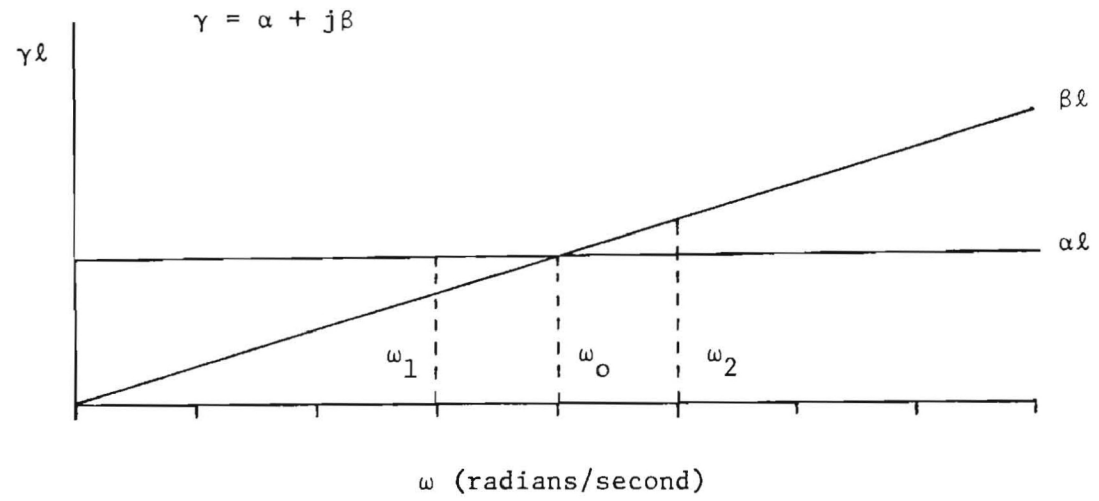

(a) Characteristics of Line Without Distortion

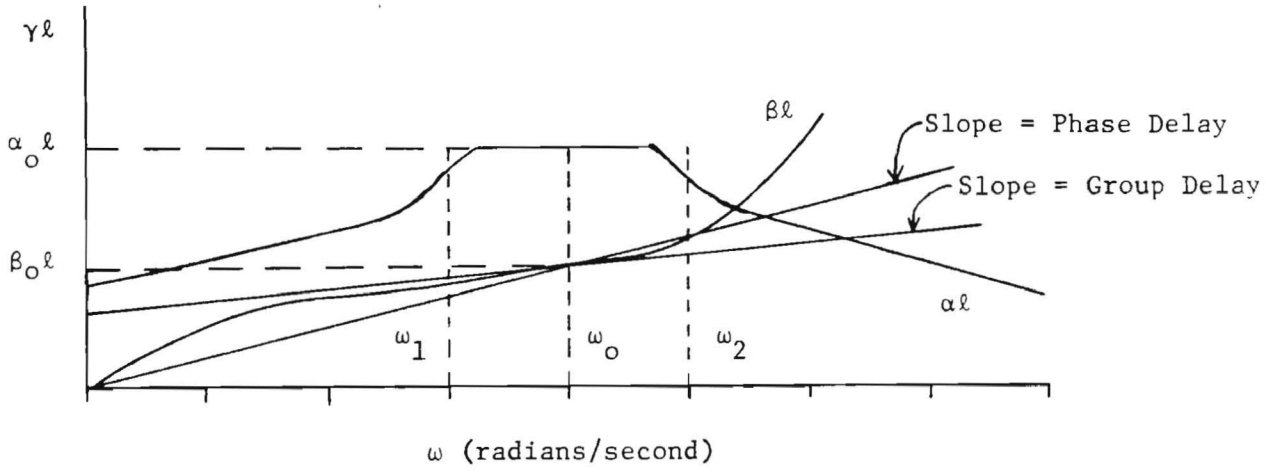

(b) Characteristics of Line With Distortion

Figure A-1 Relationship of Distortion to Group and Phase Delays

The group delay (sometimes referred to as envelope delay) of a transmission line is defined as:

$$t_g = \frac{\partial \beta \ell}{\partial \omega} \text{ seconds.} \qquad \text{(A-4)}$$

Since the group velocity is equal to

$$v_g = \frac{\partial \omega}{\partial \beta} \text{ meters/second,} \qquad \text{(A-5)}$$

the group delay expressed in terms of the group velocity is:

$$t_g = \frac{\ell}{v_g} \text{ seconds.} \qquad \text{(A-6)}$$

For a distortionless transmission line, the phase characteristic is linear and has a constant slope. Thus the phase delay is equal to the group delay for the distortionless line.

Now consider a transmission line that has distortion or is dispersive. For a dispersive line the phase velocity changes with frequency. In this case the individual sinusodial components of a complex wave will shift in relative phase as they move down the line, i.e., some components will move faster than others. At some point on the line, the sinusoidal components may add to produce a wave shape quite different than the input wave shape. Thus for large line dispersion, it may be impossible to state a single velocity describing the propagation of a wave since the signal composite changes shape as it travels. However, if there is little dispersion over the frequency band of interest, the group delay is a useful concept.

Consider the characteristic of a line with distortion shown in Figure A-1(b). The characteristic is not linear with frequency, but the loss is constant over the bandwidth. The phase delay is the slope of a line from the origin to the point (ω_o, β_o). The group delay is the slope of the characteristic at the same point. Obviously, the group delay and phase delay are not equal. If the loss, $\alpha\ell$, characteristics vary rapidly with the bandwidth, a group velocity can be defined, but it will not represent the velocity of the signal composite. So, the group delay does not always have physical meaning unless certain conditions are met.

Reflections on a transmission line change the group delay, since the reflections combine with an incident signal to change the signal composite. The effects of reflections can be seen from Figure A-2. The group delay was measured through a low-pass filter with various loads. For a 1.0 VSWR load (50 ohms) the group delay is constant when well within the band. Within the skirt region of the filter, the group delay is not constant indicating dispersion. When the load is changed to a 1.5 VSWR or a 2.0 VSWR load, the group delay changes and is not constant. Thus the minimization of reflections is an important consideration in the design of a delay line.

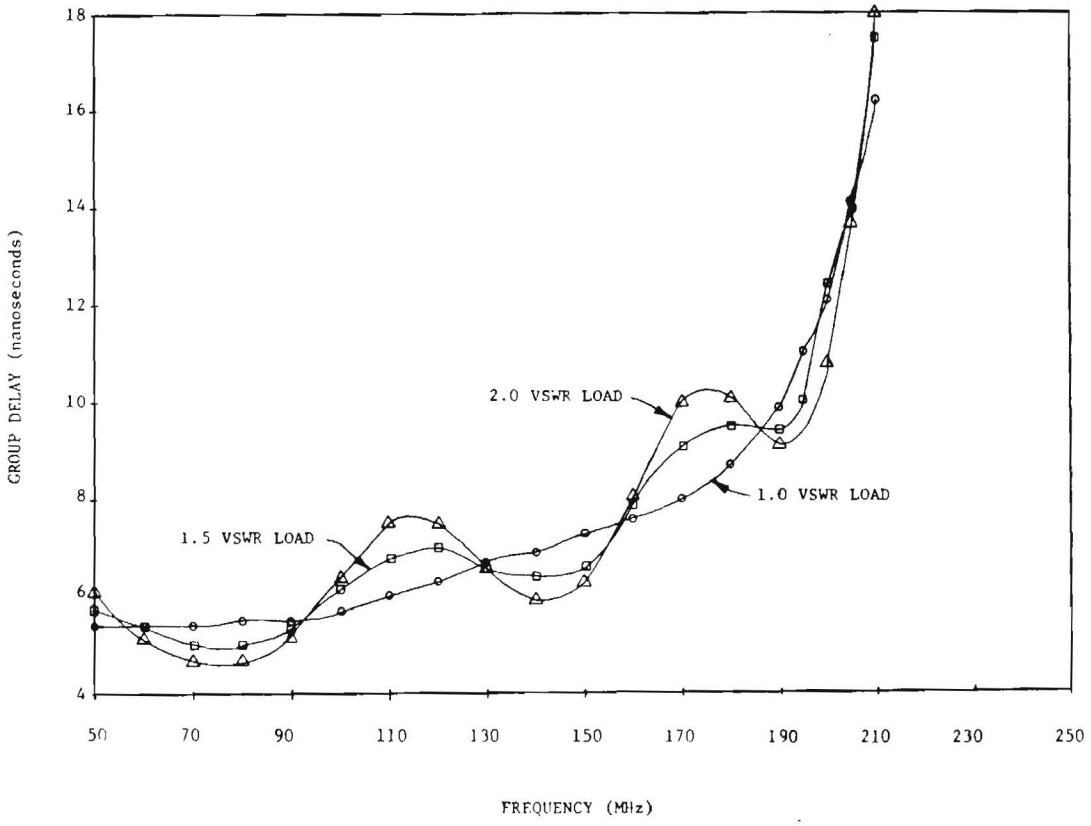

Figure A-2. Group Delay of 230 MHz Low-Pass Filter with Various Loads

APPENDIX B

MEASUREMENT INSTRUMENTATION

B.1 INTRODUCTION

The test instrumentation and procedures used to measure the characteristics of the ferrite-loaded helical line and the coupled helical line are discussed in this Appendix. Many of the measurements were common to both lines while other measurements were not.

B.2 TIME DELAY

Group delay was measured in accordance with the procedures set forth in Hewlett-Packard's Application Note 91*. The instrumentation is depicted in Figure B-1. The vector voltmeter, HP 8405A, measures both amplitude and phase through the channel A and B probes. The power splitter and pads balance and isolate the probe signals.

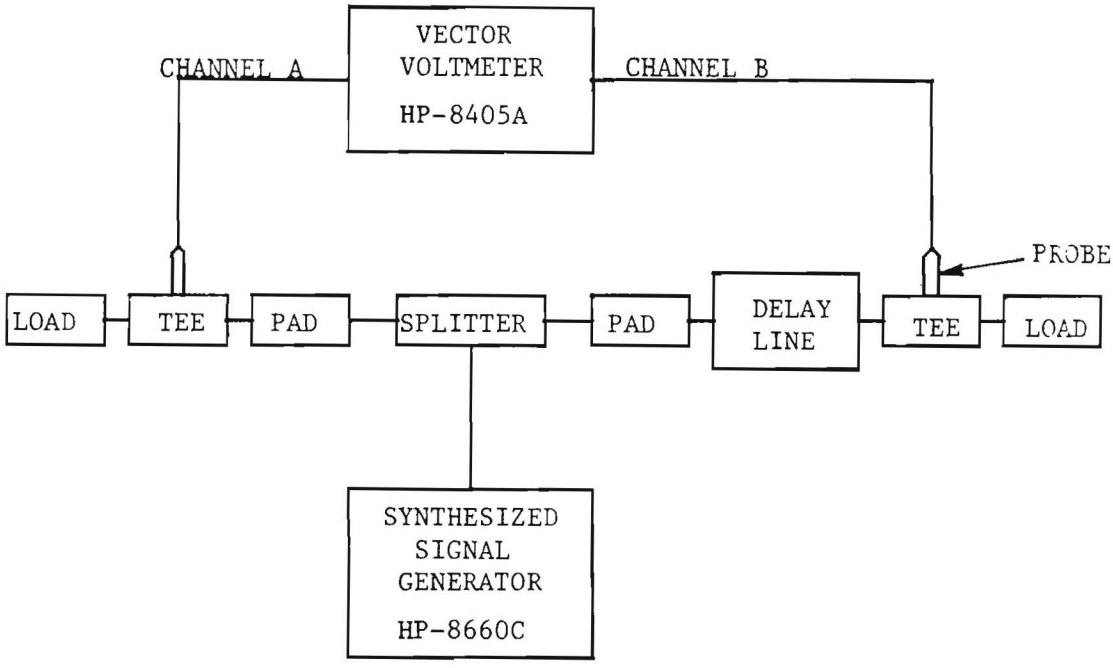

Figure B-1. Instrumentation for Measuring Time Delay and Insertion Loss

*"How Vector Measurements Expand Design Capabilities - 1 to 1000 MHz", January 1968.

The group delay (see Appendix A) is defined as:

$$t_g = \frac{\partial \phi}{\partial \omega} = \frac{\Delta \phi}{\Delta \omega} = \frac{\Delta \phi}{360 \Delta f} \qquad \text{(B-1)}$$

where

Δf = frequency change in MHz

$\Delta \phi$ = phase change in degrees.

If $\Delta f = 2.778$ MHz, the group delay in nanoseconds is equal to $\Delta \phi$. In general, group delay can be determined by changing the frequency in increments of $2.778 \cdot 10^n$ KHz and determining the group delay from the corresponding vector voltmeter changes with scale factors of 10^{-n} microsecond/degree, where n = 0, 1, 2, - - - -. The synthesized signal generator in Figure B-1 was set at a test frequency and stepped in a known frequency increment to find the group delay. This method of measuring group delay was verified using a Tektronix 3S76 sampling scope. The scope was not used for the group delay measurements since the desired resolution, particularly in the HF band, could not be obtained.

The phase delay (see Appendix A) was measured by noting the phase shift at each test frequency and using the equation:

$$\frac{t_p}{\Delta \phi} = \frac{T}{360} \qquad \text{(B-2)}$$

where

t_p = phase delay in seconds

$\Delta \phi$ = phase shift in degrees

T = period of signal in seconds.

B.3 INSERTION LOSS

The insertion loss was also measured using the instrumentation in Figure B-1. With the delay line removed, the channel A and B ratio is unity. (Actually, for some frequencies this was not the case and correction factors

were measured). When the delay line is present, the ratio of channel A to Channel B signal is the insertion loss of the delay line. The vector voltmeter displays this ratio directly in dB.

B.4 VOLTAGE STANDING WAVE RATIO (VSWR)

The VSWR was measured in accordance with the procedures set forth in Hewlett Packard Application Note 77-3*. The instrumentation is shown in Figure B-2. Basically, the vector voltmeter was used to measure the ratio of the incident signal to the reflected signal to find the reflection coefficient. The VSWR was then calculated from the equation:

$$\text{VSWR} = \frac{1 + |\rho|}{1 - |\rho|} \qquad \text{(B-3)}$$

where $|\rho|$ is the magnitude of the reflection coefficient.

B.5 IMPEDANCE

The impedance measurements were made using an HP 4815A RF Vector Impedance Meter. This instrument measures directly the impedance as a function of frequency.

B.6 POWER-HANDLING CAPABILITY

The power handling capability was determined with the instrumentation setup shown in Figure B-3. The power oscillator has a maximum output of 50 watts. The power oscillator output power was first calibrated with the delay line removed.

The power oscillator was operated at 50 watts average power, and its power was monitored using the 30 dB, 20 watt attenuator (the attenuator was air-cooled) and the power meter. After the power oscillator and attenuator had temperature stabilized, the delay line was inserted. The power oscillator was adjusted to account for the delay line insertion loss. With the delay line in place, the power was monitored on the power meter so as to note any change in insertion loss as the delay line dissipated heat.

---

*"Measurement of Complex Impedance - 1 to 1000 MHz", April 1967.

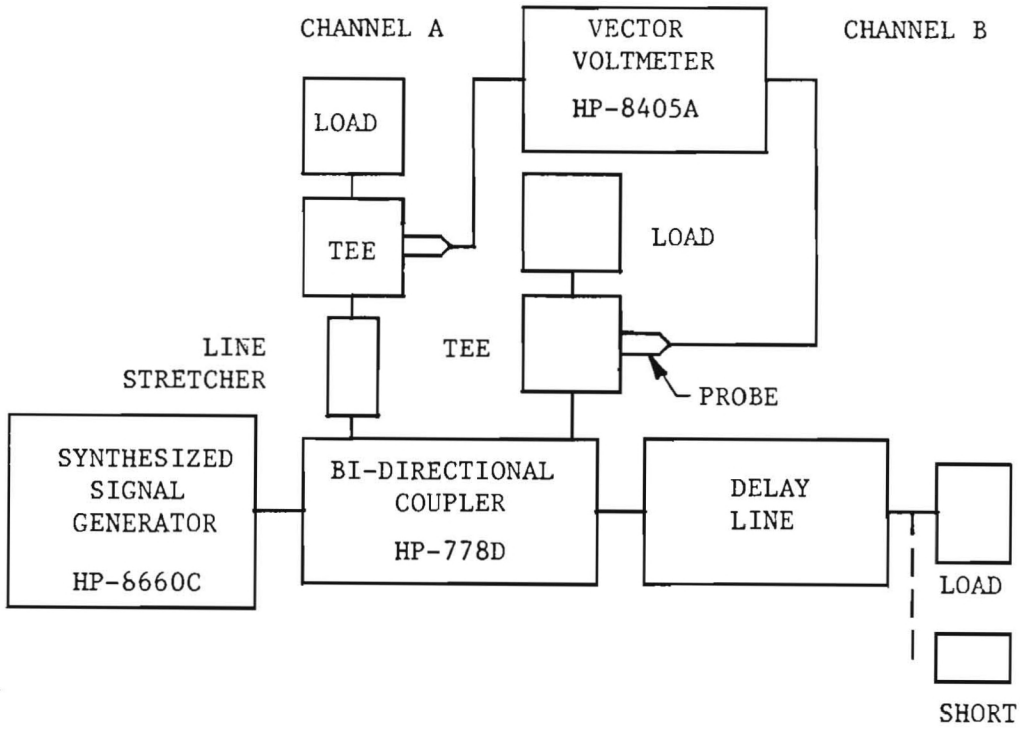

Figure B-2. Instrumentation for Measuring VSWR

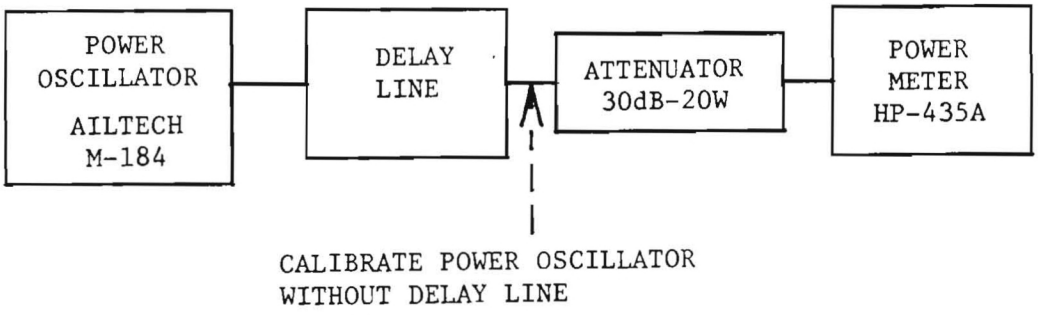

Figure B-3. Power-Handling Capability Measurements

B.7 INTERMODULATION PRODUCTS

Figure B-4 shows the instrumentation used to determine the intermodulation products. Basically, two high-power signals f_1 and f_2 were combined through a hybrid junction (which was air-cooled). Next the signals were filtered through a Sierra low-pass filter with a 44 MHz cut-off frequency. With this configuration, no intermodulation products were present at the test frequencies as long as f_1 and f_2 signals were separated by at least 5 MHz. The tuned power amplifier pass band was not sharp enough to provide adequate isolation for signals closer in frequency.

The intermodulation products of the delay line were measured on the spectrum analyzer by noting amplitude and frequency.

B.8 MAGNETIC FIELD CALIBRATION

The magnetic field used to change the time delay of the ferrite-loaded helical line was generated using solenoids. The relationship between the solenoid current and the resulting magnetic field was calibrated using a Bell Model 620 gaussmeter with a Hall Effect probe. The magnetic field at the end face of the solenoid was measured and then corrected to the solenoid center using the equation:

$$H_c = \frac{2H_e \sqrt{R^2 + \ell^2}}{\sqrt{4R^2 + \ell^2}} \qquad \text{(B-4)}$$

where H_c = magnetic field at solenoid center
H_e = magnetic field at solenoid end
R = solenoid radius
ℓ = solenoid length.

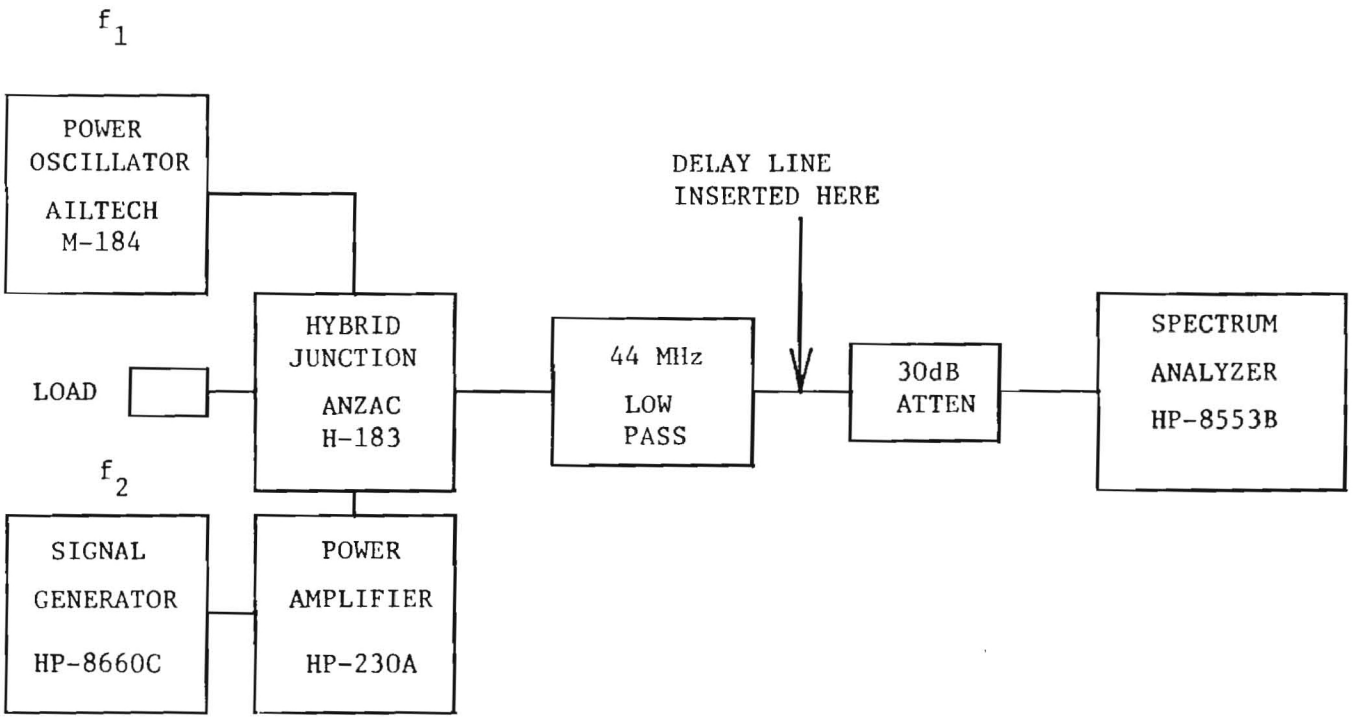

Figure B-4. Instrumentation for Intermodulation Measurements